TABLE 3-VII.- APOLLO ORBITAL SCIENCE SUMMARY

Experiment/objective	Experiment number	Mission								
		8	9	10	11	12	14	15	16	17
Bistatic radar experiment	S-170						X	X	X	
S-band transponder experiment	S-164									
CSM/LM							X	X	X	X
Subsatellite								X	X	
Infrared scanning radiometer experiment	S-171									X
Lunar sounder experiment	S-209									X
[a]Particle shadows/boundary layer experiment	S-173							X	X	
[a]Magnetometer experiment	S-174							X	X	
Cosmic ray detector (helmets)	S-151	X				X				
Apollo window meteoroid	S-176						X	X	X	X
Gamma-ray spectrometer experiment	S-160							X	X	X
X-ray fluorescence experiment	S-161							X	X	
Alpha-particle spectrometer experiment	S-162							X	X	
Mass spectrometer experiment	S-165							X	X	
Far ultraviolet spectrometer experiment	S-169									X
Lunar mission photography from the command and service module	—	X								
Lunar multispectral photography	S-158					X				
Candidate exploration sites photography	—					X	X			
Selenodetic reference point update	--					X	X			
Transearth lunar photography	—						X			
[b]Service module orbital photographic tasks	--							X	X	X
Command module orbital science photography	—						X			
Visual observations from lunar orbit	—							X	X	X
Gegenschein from lunar orbit experiment	S-178						X	X	X	
Ultraviolet photography - earth and moon	S-177							X	X	
Dim light photography	—						X			
Command module photographic tasks	--							X	X	X

[a]Particles and fields subsatellite experiments.

[b]Included panoramic camera photography, mapping camera photography and laser altimetry. Also supported geology objectives.

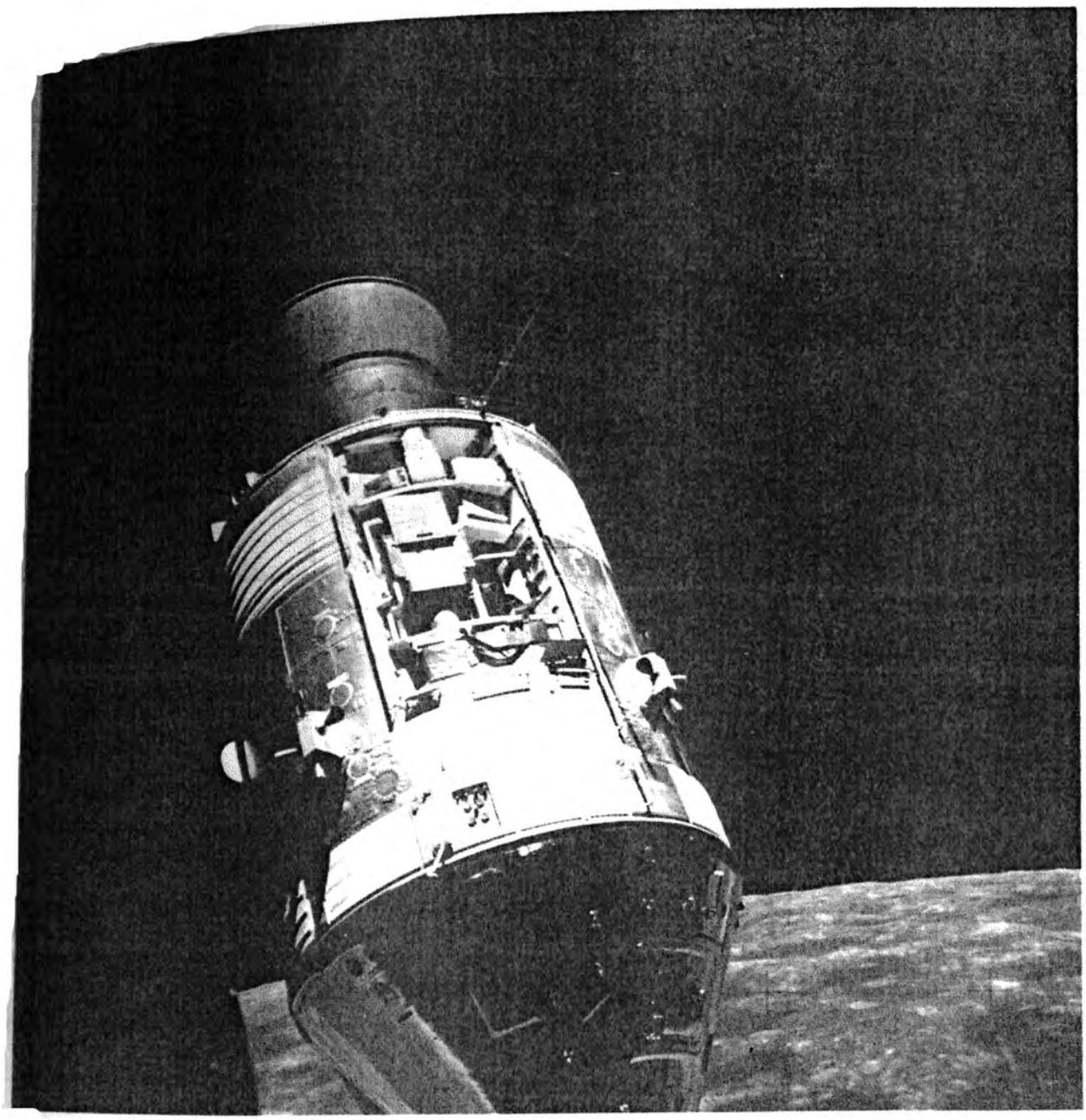

Figure 3-27.- Scientific instrument module bay viewed from the lunar module.

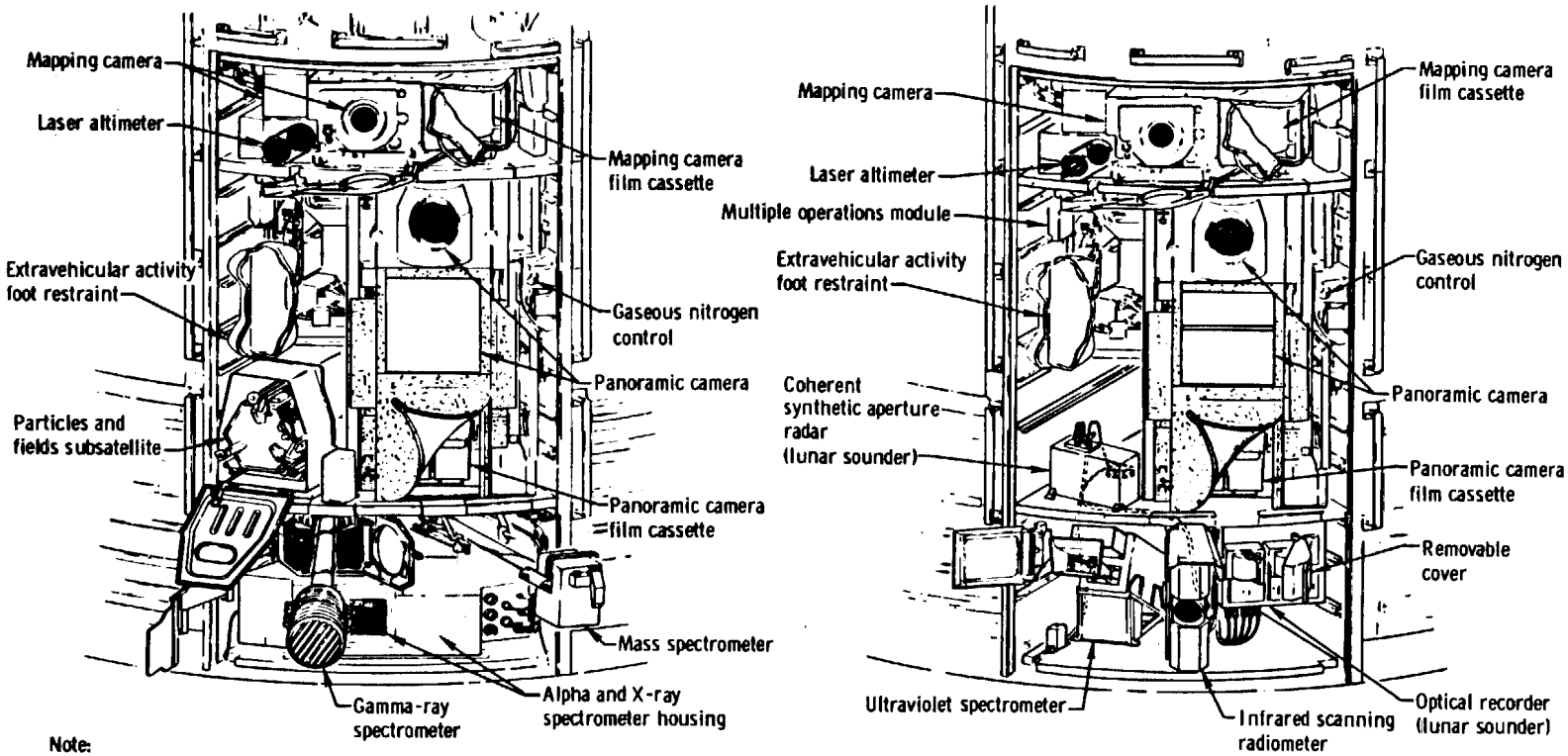

Note:
Mass spectrometer and gamma-ray spectrometer are shown partially deployed.
Some protective covers are not shown.

(a) Apollo 15 and 16 configuration

(b) Apollo 17 configuration

Figure 3-28. - Scientific instrument module configurations.

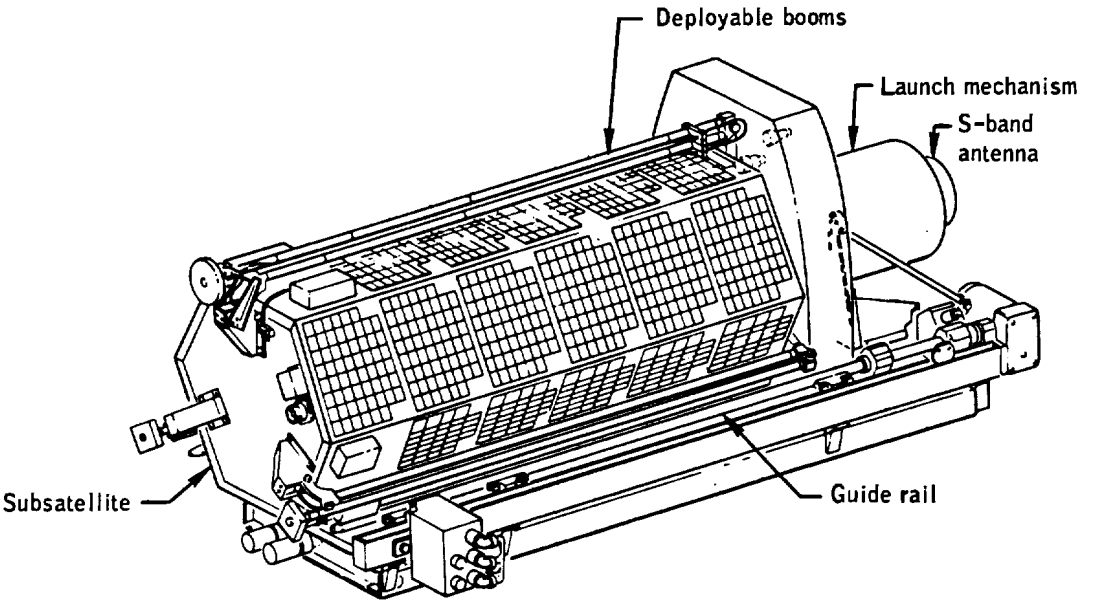

(a) Subsatellite predeployment configuration

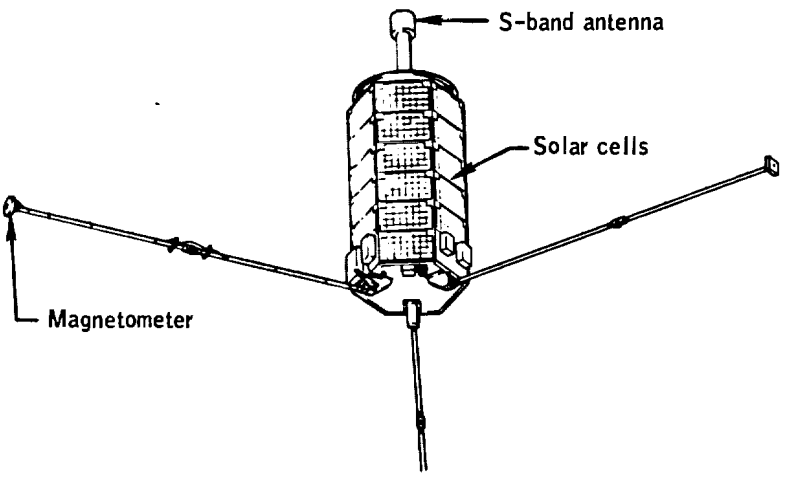

(b) Deployed subsatellite

Figure 3-29.- Subsatellite.

On the Apollo 14 mission, observations were conducted using the S-band and VHF systems simultaneously on nearly one-third of a near-side pass, and with the VHF system alone during four complete near-side passes. Good data were obtained during all observational periods. Echoes received at antennas of the earth monitoring stations were of predicted strength with signal frequency, phase, polarization, and amplitude being recorded. Comparison of the received echoes with the known characteristics of the transmitted signal yielded quantitative information about lunar crustal properties such as dielectric constant, average slope and slope probability, and small-scale surface roughness. Effects of bulk surface electrical properties such as the Brewster angle were clearly visible at both the S-band and VHF frequencies. Comparisons of radar experiment results with interpretive geologic maps and quantitative topographic work using, primarily, photogrammetric techniques showed excellent agreement.

The radar experiment configuration for the Apollo 15 mission differed from that of the Apollo 14 mission in that the S-band high-gain antenna was used instead of the S-band omnidirectional antenna system. This change resulted in a significant improvement in the quality of both S-band and VHF data. Simultaneous S-band and VHF observations were successfully conducted during one complete near-side pass, and VHF data were obtained during four complete near-side passes. Excellent data were received during these five observation periods, representing nearly an order-of-magnitude improvement in the signal-to-noise ratio with respect to the Apollo 14 experiment. For the first time, bistatic radar data were received from significant lunar features which included the Sea of Serenity, the Apennine Mountains, the middle portion of the Ocean of Storms, and the Marius Hills. The S-band data analysis indicated that the area surveyed during the Apollo 15 mission is largely homogeneous and very similar to the regions sampled at lower altitudes during the Apollo 14 mission. Although distinct variations in centimeter-to-meter-length slopes exist, the vertical structure of the surface appeared remarkably uniform.

The Apollo 16 experiment configuration was the same as that for Apollo 15. Simultaneous S-band and VHF observations were conducted during one complete near-side pass, and VHF data observations were made on four complete near-side passes. Although the S-band data received were of excellent quality, the VHF echoes were weak due either to a command and service module attitude problem or to an inflight equipment malfunction. Another problem was interference from NASA satellite TETR-D, originally launched for Apollo communication system testing and training exercises.

Results of data reduction and analyses for all three missions reveal that the oblique geometry scattering properties of the moon's surface are wavelength-dependent in the decimeter-to-meter range, that the scattering law is highly dependent on local topography, and that systematic differences exist in the average scattering properties of mare and highland units. At 13 centimeters, the reflectivity of mare surfaces is remarkably uniform except for local deviations associated with specific features; the 116-centimeter results are frequently in sharp contrast with those at the shorter wavelength. The highlands ejecta south of Mare Crisium (Sea of Crises) exhibit a dielectric constant of about 2.8 at the 116-centimeter wavelength and a lower value at the 13-centimeter wavelength. In the Apennines and central highlands, both wavelengths show a reduced reflectivity consistent with a dielectric constant decrease from 3.1 to 2.8.

The 116-centimeter variations that do not correlate with the 13-centimeter data cannot be caused by surface effects because such effects would also be observed at the shorter wavelength. Explanation of the differential behavior, in some cases, requires layering or an inversion of density with depth such as might be produced by a flow over older regolith.

Apollo 14 observations suggest that the upper 5 to 50 centimeters of the crust must be extremely uniform over the surface of the moon or that the change with depth must be gradual. Surface-modifying processes have apparently acted to these depths along the major portion of the radar groundtracks. Further, the 116-centimeter data suggest that there must be large variations (on the order of 2 to 1) in impedance contrast within 1 to 10 meters of the surface. Variation in depth of a thin regolith or covering blanket is one obvious candidate to model this effect.

The root-mean-square slopes deduced from the Apollo 14 and 15 spectra exhibit very systematic behavior with respect to maria, highlands, and discrete features such as craters. Typical highland slopes are in the range of 5 to 7 degrees at both wavelengths suggesting that, on the scale lengths of 30 to 300 meters, the surface has equal roughness. Within the maria, the 13-centimeter slopes are typically within 2 to 4 degrees, but those obtained at 116 centimeters are only half as large (ref. 3-38).

3.3.2 S-Band Transponder

The S-band transponder experiment was successfully conducted during the Apollo 14, 15, 16, and 17 missions. On all four missions, experiment data were derived from the lunar-orbiting command and service module and lunar module. In addition, the experiment was supported during the Apollo 15 and 16 missions by an S-band transponder mounted in the subsatellites that were launched from the command and service modules into lunar orbit. The purpose of the experiment was to measure the lunar gravitational field which, in turn, provided information on the distribution of lunar mass and its correlation with surface features such as craters, mountains, and maria.

No instruments were required on the command and service modules and lunar modules other than the existing S-band communications systems. A transponder system designed specifically for the experiment was contained in the two subsatellites. These systems operated in conjunction with the earth-based radio tracking system. Experiment data consisted of variations in spacecraft speed as measured by the tracking system. However, these line-of-sight velocity measurements could be obtained only while the spacecraft were in view of the earth. Information about the far side gravity field must therefore be indirectly inferred from spacecraft conditions immediately after lunar occultation and over many revolutions.

Good command and service module and lunar module data were obtained despite some degradation resulting from a high-gain antenna problem during the Apollo 14 mission and spacecraft attitude instability during the Apollo 15 and 16 missions due to reaction control system thruster attitude control firings. Both the Apollo 15 and Apollo 16 subsatellites provided excellent quality tracking data until May 29, 1972, when the Apollo 16 subsatellite crashed on the moon; the Apollo 15 subsatellite continued to provide tracking data until August 23, 1973.

In general, comparison of tracking data from the three spacecraft and from lunar areas overflown on more than one mission shows close agreement in the results. The following general conclusions have been drawn from reduced data (refs. 3-39 and 3-40).

a. All unfilled craters and those having diameters less than 200 kilometers are negative anomalies (negative gravity regions); Ptolemaeus Crater is an example of the latter type.

b. Filled craters and circular seas with diameters greater than about 200 kilometers are positive anomalies (positive gravity regions), or are mascons. The smallest of this type is the crater Grimaldi, which has a diameter of 150 kilometers; an exception is the unique Sinus Iridum (Bay of Rainbows).

c. The largest mascons detected are in the region of the Sea of Nectar, the Sea of Serenity, and the Sea of Crises. Part of the central highlands appears as a positive anomaly, and mountain ranges observed thus far (Marius Hills and Apennine Mountains) are positive anomalies.

3.3.3 Infrared Scanning Radiometer

Accomplished successfully during the Apollo 17 mission, the infrared scanning radiometer experiment obtained thermal emission measurements of the lunar surface for use in developing a high-resolution temperature map of the lunar surface. The experiment instrument, located in the scientific instrument module, operated normally throughout the mission, and all mission objectives were achieved.

Infrared radiometer data were obtained for 100 hours in lunar orbit during which time about 30 percent of the lunar surface was scanned. Approximately 100 million temperature measurements were obtained over the full lunar temperature range of 80° to 400° K. Temperature resolution was 1° K with a precision of about ±2° K; spatial resolution was approximately 2 kilometers over most of the horizon-to-horizon scan. The experiment was also operated for 10.5 hours during transearth coast to support a study of the contamination environment in the vicinity of the spacecraft.

Data analyses disclose that the nighttime cooling behavior of the moon varies. The Ocean of Storms shows a substantial number of thermal structure variations, ranging from large crater anomalies to small-scale features below the instrument resolution of less than 2 kilometers. Far fewer thermal features are evident in other areas along the spacecraft lunar surface ground-track; in particular, only a few anomalies are revealed by nighttime scans of the lunar far side. Although cold anomalies are evident throughout the data, they are usually small features which may represent indigenous activity geologically recent in time. Additional information may be found in reference 3-41.

3.3.4 Lunar Sounder

The lunar sounder experiment, flown on the Apollo 17 mission, obtained electromagnetic soundings of the moon for use in developing a selenological three-dimensional model to a depth of about 1.3 kilometers. The equipment was installed in the service module and consisted of a coherent synthetic aperture radar, the associated antennas, and an optical recorder. The radar system operated in the two HF bands of 5 megahertz (HF 1) and 15 megahertz (HF 2), or in the VHF band of 150 megahertz, and transmitted a series of swept frequency pulses. A small part of the pulse energy was reflected from the lunar surface and subsurface features and subsequently was detected by a receiver on the spacecraft. The radar video output from the receiver was recorded by the optical recorder on film, and the film cassette was retrieved during transearth extravehicular activity.

Experiment data were obtained in lunar orbit for 10 hours. The HF 1, HF 2, and VHF data were collected during six complete revolutions (two for each frequency band) and from specific lunar targets. The instrument was operated in the receive-only mode on both the lunar near side and far side, and near the landing site with and without transmission of signals by the surface electrical properties experiment deployed on the lunar surface. The experiment was also operated in the receive-only mode for 24 hours during transearth coast to determine sources of terrestrial noise.

Several experiment hardware anomalies occurred during the mission. The most serious was failure of the VHF echo tracker to keep the leading edge of the return signal on film; as a result, nadir return from both mare and highlands (and thus, sounding capability) was lost up to 50 percent of the time. Sounding data were also limited because the HF 2 channel energy was down 10 to 20 decibels relative to the HF 1 channel, as compared to premission values of 7 to 8 decibels. In addition, operational delays were caused by a faulty antenna extension/retraction mechanism and talkback indicator (attributed to low temperatures); however, neither data quantity nor quality was lost.

The VHF images produced by optical processing were of excellent quality and the VHF profile, where available, was quite satisfactory for addressing local selenomorphological problems. Tentative subsurface returns have been identified in both the HF 1 and VHF channels. Based on preliminary analyses, the data appear to have satisfied experiment requirements. Telemetry monitoring of average reflected power indicated that the mare and highlands exhibited markedly different reflectivity for both HF and VHF radar frequencies. Data were consistent with distinct layering in the mare as would be expected were the mare flooded by successive layers of lava; predicted topographic signatures over features such as craters and mare ridges have been confirmed in principle. A preliminary scan of a limited length of film indicates that both the radar images of lunar surface at the VHF frequency and the echoes delayed in time relative to the surface echo at the HF frequencies have been imprinted on film.

Preliminary data analyses also reveal that the power levels of VHF- and HF-reflected signals were very close to those predicted from premission system analyses and the known dielectric constant of the lunar surface. Electromagnetic radiation from earth in the HF 2 mode is much stronger than expected but does not appear to have degraded the active radar sounding of the lunar near side. Earth radiation is occulted by the moon and can be minimized by proper orientation of the radar antenna. Additional preliminary results are given in reference 3-42.

3.3.5 Particle Shadows/Boundary Layer

The instruments for the particle shadows/boundary layer experiment were installed in the subsatellites launched into lunar orbit during the Apollo 15 and Apollo 16 missions. The instruments in each subsatellite consisted of two silicon nuclear particle telescope detectors and four spherical electrostatic analyzer detectors. The objectives of the experiment were to describe the various plasma regimes in which the moon moves, to determine how the moon interacts with the plasma and magnetic fields in the environment, and to determine certain features of the structure and dynamics of the earth magnetosphere.

Shortly after launch of the Apollo 15 subsatellite in lunar orbit, an inconsistency was noted in the particle experiment count data. This was traced to a design error. The data were not lost, but data reduction was more complex. The design error was corrected in the Apollo 16 subsatellite. Failures of the Apollo 15 subsatellite on February 3 and February 29, 1972, resulted in the loss of most operational and experiment data. As noted in section 3.3.7, the Apollo 16 subsatellite impacted the lunar surface after orbiting for approximately 1 month. During its lifetime, however, it provided excellent quality data.

Data were obtained as the subsatellites encountered four distinct regions of magnetized plasma (fig. 3-30): the solar wind; the bow shock, which appears on the sunward side of the earth magnetosphere; the magnetosheath, which lies between the bow shock and the earth magnetosphere; and the magnetotail. In addition to the plasma and energetic particle characteristics of these regions, particles from the sun also appear after chromospheric flares occur or active centers pass across the solar disk. Results from the Apollo 15 and 16 experiments essentially agree (refs. 3-43 and 3-44). The findings are summarized as follows.

a. A wide variety of particle shadows has been measured; the shadow shapes agree well with the theory that has been developed and verify that the magnetotail magnetic field lines are generally "open" in the sense that they connect directly from the earth polar caps to the interplanetary magnetic field.

b. The cavity formed in the solar wind by the moon has been observed in the fast-electron component of the solar wind. When the interplanetary magnetic field is aligned approximately along the solar wind flow, the electrons are almost completely excluded from the cavity. When the magnetic field is aligned more nearly perpendicular to the solar wind flow, the solar wind shadow structure (as defined by the fast-electron component) becomes extremely complex. The shadow structure becomes much broader than the lunar diameter and may become very shallow.

c. A weak flux of electrons in the energy range of 25 000 to 300 000 electron volts was able to move predominantly in a sunward direction for a period of several days while the moon was upstream from the earth in interplanetary space. No determination has been made as to whether these particles have a solar or terrestrial origin.

d. Flux of solar electrons was measured after two important solar flares occurred. An electron spectrum for the energy range of 6000 to 300 000 electron volts was determined from Apollo 15 measurements of the first flare that occurred on September 1, 1971. After a major hydromagnetic shock wave that was generated on May 15, 1972, the Apollo 16 experiment measurements indicated that fluxes of electrons at energies above approximately 2000 electron volts increased by more than an order of magnitude above background levels; energetic proton fluxes throughout the event were typically higher than electron fluxes at the same energy by a factor of 10.

e. Magnetotail electric fields have been determined from particle shadow boundary displacements. Their magnitude ranges from zero to more than 1 volt per kilometer, typically, 0.2 to 0.3 volts per kilometer, oriented in a generally east-to-west direction, indicative of solar wind induction driven convection toward a magnetic neutral line merging region in the center of the magnetotail.

f. Low energy electron fluxes characteristic of the plasma sheet observed by satellites passing through the magnetotail nearer the earth are also frequently observed from lunar orbit. The location of plasma sheet encounters appears to be less closely confined to regions near the magnetic neutral sheet (field reversal region) than is observed closer to the earth.

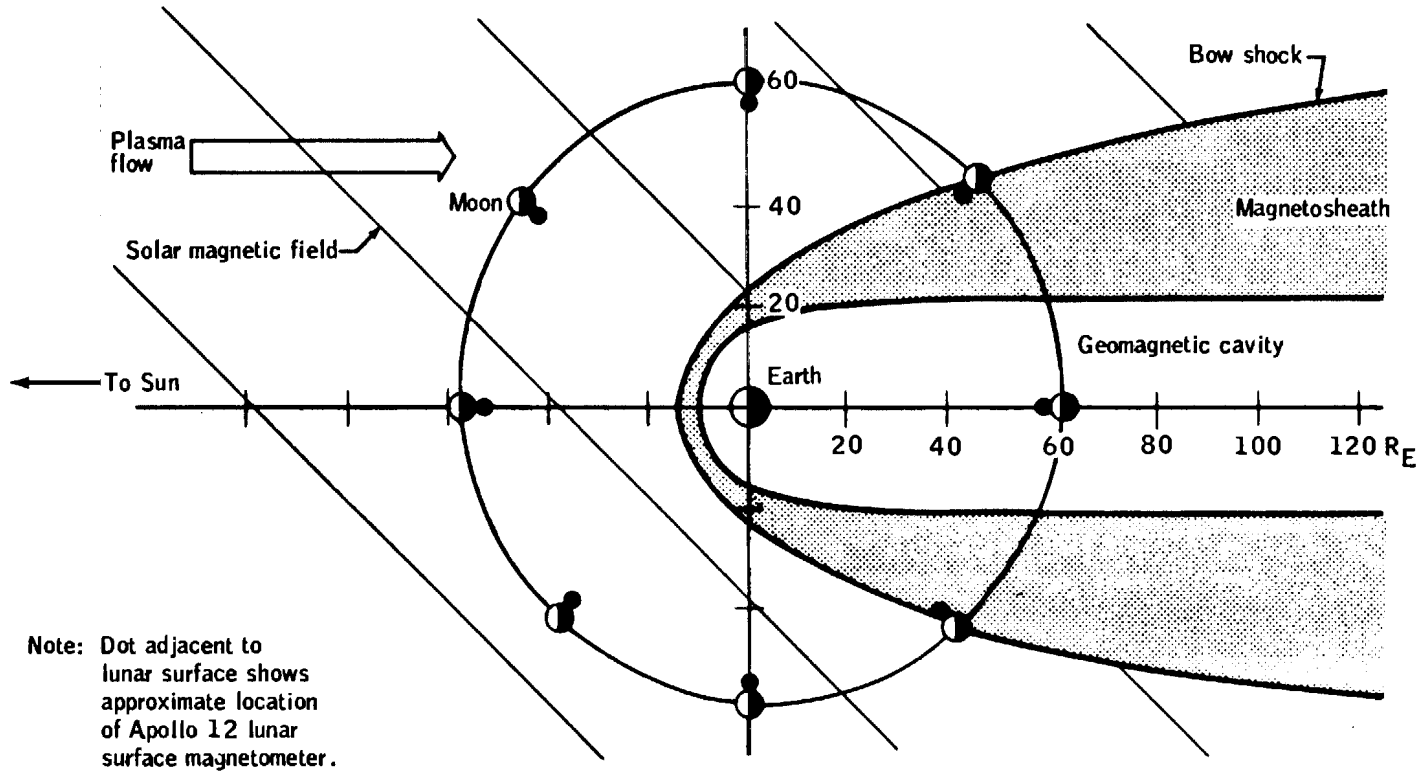

Figure 3-30.- Near-earth space traversed by moon.

g. Areas are observed to exist where 15 000-electron-volt electrons are reflected back to the spacecraft from the direction of the moon, probably by regions of remanent surface magnetism of sufficient magnitude to exceed the "mirroring" value for electrons.

3.3.6 Magnetometer

A biaxial flux-gate magnetometer was also included in the Apollo 15 and Apollo 16 subsatellites to calculate the interior electrical conductivity of the moon, to survey the remanent magnetization of the lunar surface, and to study the interaction of the moon with its plasma environment. The magnetometer was boom-deployed from the subsatellite and measured the magnitude and polarity of two mutually orthogonal vector components, one parallel and the other perpendicular to the spin axis of the subsatellite. Experiment results (refs. 3-45 and 3-46) are summarized in the following paragraphs.

Data obtained in the magnetotail by the Apollo 15 and Apollo 16 experiments show that lunar remanent magnetism can be mapped from a single orbiting vehicle. However, high-resolution maps of magnetic features can be achieved only with dual magnetometer surveys in order to separate temporal and spatial changes in the fields, or with low-altitude data below 70 kilometers. The latter data are available from the Apollo 15 and Apollo 16 missions only for limited areas. Although the character of the magnetic features observed tends to follow the character of the lunar topography beneath the subsatellite, there is no one-to-one correlation of magnetic signature with surface features.

The approximate nature of this correlation was shown by constructing a high-resolution contour map of lunar contribution to the solar-directed component of the magnetic field as measured on the Apollo 15 subsatellite at an altitude of 67 kilometers in the Van de Graaff region. The map shows a well-defined feature with a 4.5 gamma peak-to-valley variation. This feature is clearly not centered over Aitken or Van de Graaff, which suggests that these magnetic features are not necessarily associated with crater formation (ref. 3-46).

The subsatellite data obtained in the solar wind indicate that diamagnetic enhancement and rarefaction dips discovered by Explorer 35 magnetometers are also distinctly present at the much lower altitude of approximately 100 kilometers. The phenomenon of large increases in the field external to the rarefaction dips is also clearly observed and appears to be stronger at the subsatellite altitude.

3.3.7 Subsatellite Performance

The two particles and fields subsatellites were launched from the Apollo 15 and 16 command and service modules and were to be operated in lunar orbit for a 1-year period.

3.3.7.1 Apollo 15.- The Apollo 15 subsatellite was launched into lunar orbit August 4, 1971, and performed satisfactorily in all modes of operation until February 3, 1972. Data were lost from about one-third of its measurements beginning on February 3, 1972, during its 2203rd lunar revolution. Data from additional measurements were lost beginning February 29, 1972, during its 2520th lunar revolution.

Analysis of the data indicated the data loss was the result of multiple failures within a single integrated circuit flatpack in the bilevel, main-frame, and drivers board of the digital electronics unit. The cause of the integrated circuit failure is not known. Following the failure, the subsatellite continued operation with the remaining particles experiment measurements, but primarily as an S-band transponder lunar gravity experiment.

The last tracking pass for the subsatellite was on August 23, 1973, on its 9046th lunar revolution. One of the requirements for the silver-cadmium battery was for a cell life for a 365-day space mission with 5000 charge/discharge cycles. The flight battery was activated in August 1971, and accumulated over 8000 charge/discharge cycles by April 1973 when it began showing charging problems and data became intermittent. This performance was in agreement with battery life predictions based on the results from the Pioneer spacecraft battery life tests. It ceased charging in August 1973 after approximately 9400 cycles.

3.3.7.2 Apollo 16.- The Apollo 16 subsatellite was launched into lunar orbit April 24, 1972, and performed satisfactorily in all modes of operation until impacting the lunar surface on May 29, 1972.

The execution of a command and service module orbit shaping maneuver had been planned before launching the subsatellite so as to place it in an orbit which would insure 1-year operation. However, the orbit-shaping maneuver was deleted because of a command and service module malfunction, and the subsatellite was placed in an orbit which was different from the one planned. The orbit into which the subsatellite was launched resulted in a short orbital life with an early impact of the subsatellite on the lunar surface.

3.3.8 Cosmic Ray Detector (Helmets)

Five helmets were used as heavy-particle dosimeters in the cosmic ray detector experiment: one worn during the Apollo 8 mission (December 21 to 27, 1968), three worn during the Apollo 12 mission (November 14 to 24, 1969); and a control helmet that was exposed to cosmic rays at a balloon altitude of 41 kilometers (July 11 and 12, 1970). After exposure, the helmets were chemically etched to reveal tracks caused by heavy cosmic ray nuclei.

Track observations show that the integrated flux of heavily ionizing cosmic rays striking Apollo 12 helmets was 3.1 times greater than that of the Apollo 8 helmet. The track formation rate for Apollo 12 helmets was 2.0 times higher than that of the Apollo 8 helmet, even when allowances were made for the differences in mission duration; the rate for the control helmet was 3.1 times higher than that of the Apollo 8 helmet and about 1.45 times higher than that of the Apollo 12 helmets. Helmet locations in the spacecraft and variations in spacecraft shielding produced no meaningful statistical differences between the track densities of the Apollo 12 helmet exposed only in the command and service module and those exposed in the lunar module and on the lunar surface. Instead, doses at the helmet depended primarily on the intensity of solar activity during the mission.

3.3.9 Apollo Window Meteoroid

The Apollo window meteoroid experiment utilizes heat shield windows from the recovered command module spacecraft (1) to obtain information about the flux of meteoroids with masses of 10^{-7} gram and less, (2) to examine the residue and morphology of the craters produced by these meteoroids for information regarding the dynamic and physical properties of the meteoroids, (3) to discover possible correlations with lunar-rock-craters studies, and (4) to obtain information on meteoroid composition and mass density.

The Apollo window meteoroid experiment was officially assigned to Apollo missions 14, 15, 16, and 17. With the exception of Apollo 11, however, the windows of all Apollo command modules have been examined for contamination and for meteoroid impact craters having diameters of 40 micrometers and larger. Contamination by hard chemical deposits was observed on the outer surfaces of all returned windows. Chemical analyses show that the contamination sources were the Mylar coating on the heat shield surface, reaction control system thruster nozzle residue, and charred heat shield material (ref. 3-47). A high percentage of sodium was produced by the thruster nozzles and heat shield char, of magnesium by thruster nozzles, and of titanium and silicon by the Mylar coating. A number of other surface effects from low-velocity particles has also been found after many of the missions, probably originating from the reaction control system thrusters and the jettison rocket of the command module launch escape system.

Approximately 3.5 square meters of Apollo window surfaces have been scanned at a general level of 20x magnification. Ten meteoroid impact craters have been found: five of these were on the Apollo 7 windows, one each on the Apollo 8, 9, and 13 windows, two on the Apollo 14 windows, and none on the Apollo 15, 16, and 17 windows. Data for craters ranging from 1 to 40 micrometers indicate that the meteoroid mass limit at the detection threshold for the 20x scan is about 10^{-11} gram. Combining these test data with previous hypervelocity data in glass targets indicates that several crater regimes exist for craters ranging from 250 micrometers to 4 centimeters: Initially, there is a hemispherical crater, typical of those in soft metal, with a lip extending around the target surface; a space zone then forms at a higher energy, removing the lip; and,

at still higher energy levels, outer space zones appear and the original hemispherical crater is ejected, leaving a conical residual crater with conchoidal ridges. The mass limit of 10^{-11} gram for the 20x scan represents a meteoroid of approximately 4 micrometers in diameter at the average meteoroid velocity of 20 kilometers per second and mass density of 2 grams per cubic centimeter.

Experiment results indicate that the flux represented by the number of observed impacts and area-time exposure is compatible with the flux estimates obtained from the results of penetration sensors mounted on the Pegasus 1, 2, and 3 satellites and on the Explorer 16 and 23 satellites; from Surveyor III data; and from a near-earth environment model. Although the extent of window contamination leaves some doubt that meteoroid composition can be positively distinguished from residue associated with each crater, the capability of this experiment to detect meteoritic residue cannot be discounted.

3.3.10 Gamma-Ray Spectrometer

Gamma-ray spectrometer instruments were flown on the Apollo 15 and 16 missions. The experiment was conducted while in lunar orbit to obtain data on the degree of chemical differentiation that the moon has undergone and the composition of the lunar surface. The equipment was also operated during transearth coast to provide calibration data on spacecraft and space background fluxes, and to provide data on galactic gamma-ray flux. A gamma-ray detector, capable of measuring gamma radiation in the energy range from 200 000 to 10 million electron volts, was mounted on an extendable boom located in the scientific instrument module. The boom could be extended 25 feet, extended to two intermediate positions, retracted, or jettisoned by the crew by using controls in the command module crew station. Controls were also provided to activate or deactivate the spectrometer, incrementally alter the sensitivity (gain) of the detector, and select either of two detector counting modes.

On the Apollo 17 mission, a sodium iodide crystal identical to those used as the detector scintillator on the Apollo 15 and 16 missions was flown as a calibration reference for interpretation of Apollo 15 and 16 data.

On the Apollo 15 and 16 missions, data were collected in lunar orbit and during transearth coast for 215.2 and 109.5 hours, respectively. Of the lunar orbital data hours, 111.8 were prime data obtained after lunar module separation from the command and service module and 103.4 were degraded by the Apollo lunar surface experiments package fuel capsule (attached to the lunar module) when the spacecraft were docked. All science objectives were satisfied on both missions in spite of the following minor anomalies: During the Apollo 15 mission, the spectrometer experienced a gain shift of approximately 30 percent. Compensation for the shift was made operationally and, by the end of the mission, the spectrometer was operating in a relatively stable state near the end of its adjustment. After transearth injection, a temporary zero-reference shift occurred, causing the first eight channels of data to be grouped into one reporting channel; however, there was no loss of experiment data. This anomaly was determined to be a one-time failure of a component and no corrective action was required for the Apollo 16 instrument. Tests conducted with the qualification unit verified that the earlier problem was caused by aging of the photomultiplier tube in the gamma-ray detector assembly as a result of high cosmic ray flux rates in lunar operation. To correct for this, the Apollo 16 flight unit was subjected to high levels of radiation, thereby aging the detector photomultiplier tube. During the Apollo 16 mission, the instrument boom mechanism stalled and would not retract fully on three of five retractions. No corrective action was taken since this mechanism was not scheduled for further use.

Analyses of the experiment data from the Apollo 15 and 16 missions relating to radioactivity levels of specific lunar surface areas are in agreement. The results of these analyses (refs. 3-48 and 3-49) are summarized as follows.

a. Regions of highest activity are the western maria, followed by the Sea of Tranquillity and the Sea of Serenity. Detailed structure exists within high-radioactivity regions. High activity observed in the Fra Mauro area during the Apollo 16 mission is at approximately the same levels as those observed around Aristarchus Crater and south of Archimedes Crater during the Apollo 15 missions. These levels are also comparable to that of the soil returned from the Apollo 14 mission.

b. Radioactivity is lower and more variable in the eastern maria. Considerably lower activity is found in the far-side highlands with the eastern portion containing gamma-ray activity lower than that found in the Ocean of Storms and the Sea of Rains by an order of magnitude. The Descartes area appears to have undergone some admixing of radioactive material.

c. Preliminary data show intensity peaks that correspond to the characteristic energies of the isotopes of iron, aluminum, uranium, potassium, and thorium.

d. Discrete, celestial gamma-ray sources were detected. These sources include the Crab Nebula, Sagittarius, local clusters of galaxies, and the super cluster that contains the Virgo cluster.

3.3.11 X-Ray Fluorescence

Identical X-ray fluorescence experiments flown on the Apollo 15 and 16 missions were used principally for orbital mapping of the composition of the moon and, secondarily, for X-ray galactic observations during transearth coast. Lunar surface measurements involved observations of the intensity and characteristic energy distribution of the secondary or fluorescent X-rays produced by the interaction of solar X-rays with the lunar surface; astronomical observations consisted of relatively long periods of X-ray measurements of preselected galactic sources such as Cyg X-1, Sco X-1, and the galactic poles.

The X-ray fluorescence experiment equipment consisted of an X-ray detector assembly capable of detecting X-rays in the energy range from 1000 to 7000 electron volts, a solar monitor, and an X-ray processor assembly. The X-ray detector assembly, located in the scientific instrument module, detected X-rays reflected from the lunar surface or emitted by galactic X-ray sources. The solar monitor, mounted in sector IV of the service module (displaced 180° from the X-ray detector assembly), measured solar X-ray flux. The measurement of fluorescent X-ray flux from the lunar surface and the direct solar X-ray flux that produces the fluorescence yielded information on the nature of the lunar surface material.

X-ray fluorescence data were collected for totals of 186.1 hours in lunar orbit (143.9 hours of prime data and 42.2 hours of degraded data) and 52.5 hours during transearth coast. Except for minor noise problems which did not adversely affect experiment data, no equipment anomalies occurred during the two missions.

Data were collected from slightly more than 20 percent of the total lunar surface, all within a band between 30° north to 30° south latitude which included some area of overlap on the two missions. Results of Apollo 15 and 16 data analyses agree closely. Confirmation of these results by analyses of lunar surface samples indicate that the X-ray method is reliable for geochemical mapping and that it can be used to determine both the major and more subtle compositional differences between lunar maria and highland areas. The following summary results of the two experiments were obtained from references 3-50 and 3-51.

a. Apollo 15 and 16 overlap regions were located between 50° to 60° east longitude, and covered such areas as the Sea of Fertility, Smyth's Sea, Langrenus Crater, and the highlands west of Smyth's Sea (fig. 3-1). Aluminum/silicon and magnesium/silicon concentration ratios in these areas, determined from Apollo 15 and 16 data, agree within 10 percent or better. Aluminum/silicon concentration ratios range from about 0.36 to 0.60 for Apollo 15 and 0.41 to 0.61 for Apollo 16; magnesium/silicon concentration ratios range from about 0.25 to 0.21 for Apollo 15 and 0.26 to 0.20 for Apollo 16.

b. The Apollo 16 data show that for areas between 9° and 141° east longitude, aluminum/silicon concentration ratios ranged from about 0.38 to 0.71, and those for magnesium/silicon from about 0.40 to 0.16. Aluminum concentrations in the mare regions are 2 to 3 times lower than in the terra and highland regions; magnesium concentrations in the mare regions are 1.5 to 2 times higher than in the terra regions.

c. Aluminum/silicon and magnesium/silicon ratios indicate that the highlands have a widespread differentiated crust having a materials composition that varies between anorthositic gabbro and gabbroic anorthosite, with probable occurrences of anorthosite, felsite and KREEP (a material rich in potassium, rare-earth elements, and phosphorous).

d. The aluminum/silicon ratios and optical albedo values correspond closely, thus establishing that the albedo is a good guide to highland composition, specifically the plagioclase content.

e. During transearth coast, X-ray data were obtained on several discrete X-ray sources and other targets dominated by diffuse X-ray flux. The behavior of pulsating X-ray stars Cyg X-1 and Sco X-1 may be characterized by quiet periods and activity periods with durations up to a day. Ten to thirty percent changes in X-ray intensity occur in a few minutes; the intensity of Cyg X-1 can double within a day or so. This increase occurs in the three energy levels measured: 1000 to 3000 electron volts, 3000 electron volts, and 7000 electron volts.

3.3.12 Alpha-Particle Spectrometer

Identical alpha-particle spectrometer experiments flown on the Apollo 15 and 16 missions were designed to map differences in uranium and thorium concentrations across the lunar surface. These differences were identified by measuring the alpha-particle emission of two gaseous daughter products of uranium and thorium, radon-222 and radon-220, respectively. Because radon itself is the product of the decay of uranium and thorium, mapping of the concentrations of these two elements can be accomplished by identifying regions of high radon activity.

The experiment equipment consisted of an alpha particle sensing assembly that could detect alpha particles in the energy range from 4.7 million to 9.1 million electron volts, supporting electronics, and temperature monitors housed in the same enclosure as the X-ray fluorescence experiment assembly. Controls were provided in the command module crew station to deploy a shield protecting the experiment detectors from spacecraft contamination sources and to activate and deactivate the experiment.

Experiment data were collected for 211.6 hours in lunar orbit (160.4 hours of prime data and 51.2 hours of degraded data) and 110.3 hours during transearth coast. No equipment anomalies occurred that required remedial action; although two of the ten detectors in the Apollo 15 instrument were noisy intermittently, data validity was not affected. The following summary of results of the experiments was obtained from reference 3-52.

a. Radon emanation from the moon was positively detected although the average level is about three orders of magnitude below terrestrial levels.

b. Several interesting characteristics in the spatial and temporal distribution of lunar radon were observed. An area of relatively high radon emanation includes Aristarchus Crater, Schroter's Valley, and Cobra Head.*

c. The most conspicuous localized feature is Aristarchus Crater where the counting rate of radon-222 alpha particles is at least four times the lunar average. Grimaldi Crater appears to be the site of another localized concentration, and the edges of the great maria basins are also sites of increased activity.

d. Transient radon emanation from the moon also occurs, based on detection of large amounts of polonium-210 (a daughter product of radon-222 and a decay product of lead-210). Polonium-210 was detected in a broad area extending from west of the Sea of Crises to the Van de Graaff-Orlov Crater region; polonium-210 levels of concentrations were much higher than required to be in equilibrium with radon-222. An area having even higher concentrations of polonium-210 is located approximately 40° east longitude and centered around the Sea of Fertility.

3.3.13 Mass Spectrometer

Objectives of the mass spectrometer experiment, flown on the Apollo 15 and 16 missions, were to measure the composition of the lunar atmosphere and to search for active volcanism on the lunar surface. These data are important to understanding the evolution of the moon and the gas transport mechanisms in other more complete planetary exospheres. Lateral transport can be observed in an idealized form in the lunar atmosphere because gas molecules do not collide with each other but, instead, travel in ballistic trajectories to form a nearly classical exosphere after encounters with the lunar surface.

*Informal designations.

The experiment assembly consisted of the mass spectrometer and its electronic components mounted on a boom which was extended 24 feet from the scientific instrument module. The instrument was capable of measuring the abundance of particles in the 12- to 66-atomic-mass-unit range. A shelf-mounted shield to protect the spectrometer from spacecraft contamination sources when in its stowed position opened and closed automatically when the boom was extended and retracted. In addition to acquiring data while in lunar orbit, the spectrometer was operated at various intermediate boom positions for specified periods during transearth coast to determine the concentration of constituents forming the so-called contamination cloud from the command and service module. Command module crew station controls were provided to extend, retract, and jettison the boom; activate and deactivate the spectrometer; select high and low spectrometer discrimination modes and multiplier gains; and control ion source heaters and filaments.

Experiment data were collected for 134 hours in lunar orbit (127 hours of prime data and 7 hours of degraded data) for both missions, and 48 hours during the transearth portion of the Apollo 15 mission. Boom retraction anomalies occurred on both missions. On the Apollo 15 mission, the boom did not fully retract on 5 of 12 occasions. On the Apollo 16 mission, the boom never fully retracted and then stalled at the two-thirds position during final retraction for the transearth injection maneuver. Because the maneuver could not be performed with the boom extended, it was jettisoned, thereby preventing collection of data during transearth coast. In the absence of specific evidence, the incomplete retractions were assumed to have been caused by jamming of the cable in the boom housing because of stiffening during periods of cold soak. The repeated and prolonged stalling of the motors on the Apollo 16 mission caused the final failure of the boom in mid-stroke. Results of data analyses (refs. 3-53 and 3-54) are summarized as follows.

Large quantities of gas were observed in lunar orbit that could neither have orginated in lunar orbit nor resulted from spacecraft direct outgassing. The plausible source of these gases is the waste liquids periodically dumped from the spacecraft. These liquids quickly freeze, forming gases into solid particles that co-orbit the moon with the spacecraft. Subsequent evaporation produced many of the gases observed.

Data were obtained on the partial pressure of neon-20. At the 100-kilometer orbital altitude, the concentration is $(8.3 \pm 5) \times 10^3$ atoms per cubic centimeter. This value translated into the nighttime surface concentration becomes $(4.5 \pm 3) \times 10^5$ atoms per cubic centimeter. The value is lower than previous estimates by approximately a factor of 3 but is in fair agreement with the data from the Apollo 14 and 15 cold cathode ionization gages operating on the lunar surface.

3.3.14 Far Ultraviolet Spectrometer

The ultraviolet spectrometer was a scientific instrument module experiment flown only on the Apollo 17 mission. The purpose of this experiment was to measure the density, composition, and temperature of the lunar atmosphere. The instrument developed for this purpose was a large and highly sensitive far ultraviolet spectrometer which scanned the spectral region of 1180 to 1680 angstroms every 12 seconds with a spectral resolution of 10 angstroms. The experiment instrument was sensitive to all possible atmospheric species except argon, helium, and neon.

The most definitive information previously obtained about the density of the lunar atmosphere was with cold cathode ion gages deployed on the lunar surface on the Apollo 14 and 15 missions. Data obtained by these gages indicated that the lunar surface is an exosphere, with the lunar surface defining the exobase and, therefore, controlling the "temperature" of the atmosphere. More specifically, the data showed that there are no collisions between the atmospheric molecules or atoms and that the sources of the lunar atmosphere are the solar wind, lunar degassing, and radiogenic gases (argon and radon) formed by lunar radioactivity.

The ultraviolet spectrometer experiment was designed to optimize the observation of atomic hydrogen and xenon by spending about 45 percent of each spectral cycle scanning the resonant emissions of these two species. Optimization for xenon detection at 1470 angstroms was planned on the basis that this heaviest of the naturally occurring gases would probably be the most resilient to the loss processes that had reduced the primordial lunar atmosphere density to at least 10^{-12} of the density at the surface of the earth.

Far ultraviolet spectral data were collected for 80 hours in lunar orbit and for approximately 60 hours during transearth coast; a solar atmospheric observation was added in real time. All planned observations were accomplished, including those of lunar atmosphere composition and density; lunar ultraviolet albedo; solar system Lyman-alpha (1216 angstroms); ultraviolet zodiacal light; and ultraviolet spectra of the earth, several stars, and extragalactic sources. Equipment performance was nominal with two minor exceptions — failure of internal temperature sensing circuits and an unexpected high background count rate attributed to cosmic background. These problems did not impair collection of data or degrade its quality. Experiment results based on preliminary analyses are summarized as follows (ref. 3-55).

a. The present results indicate that the lunar surface concentration of atomic hydrogen is less than 10 atoms per cubic centimeter, almost three orders of magnitude less than predicted. This is consistent with the hypothesis that the solar wind protons are completely converted into hydrogen molecules at the lunar surface. The fact that xenon must be at best a minor component of the lunar atmosphere, despite its large mass, indicates that the mechanism of photoionization loss followed by acceleration in the solar wind electric field dominates over Jean's evaporative escape, at least for the heavy gases. The small concentrations of hydrogen, carbon nitrogen, oxygen, and carbon monoxide, which are photodissociation products of many gases of volcanic origin, also place severe restrictions on present levels of lunar volcanism.

b. Lunar albedo measurements confirm those made on lunar samples from the Apollo 11, 12 and 14 missions.

c. Information was obtained on ultraviolet zodiacal light emissions from the inner solar atmosphere. These data generally support the ultraviolet zodiacal light observations by Orbiting Astronomical Observatory 2.

d. During transearth coast, data were collected on stellar and extragalactic sources, and a general ultraviolet survey of the sky was conducted. Preliminary analysis of the spectra of isolated bright stars demonstrates that significant data were obtained. The observed ultraviolet spectral distributions agree with previous observations and provide the most precise measurement of the absolute ultraviolet brightness obtained to date.

3.3.15 Lunar Mission Photography From the Command and Service Module

Photographs of the lunar surface were taken from the command module on the Apollo 8 mission primarily for geodetic and operational purposes. The principal objectives were to obtain overlapping or stereoscopic-strip photographs, to photograph specific targets of opportunity, and to photograph a potential landing site through the sextant.

Approximately 90 percent of the objectives were met despite curtailment of photographic activities toward the end of the lunar orbit period because of crew fatigue and spacecraft operational requirements. The results were as follows:

a. Excellent coverage was obtained of selected areas on the far side of the moon complementing near-side photographs taken during the Lunar Orbiter series. Photographs were taken through the entire range of sun angles, and revealed albedo variations not previously detected as well as many bright-rayed craters ringed with high-albedo material.

b. Vertical and oblique stereoscopic photographs between terminators were obtained with the 70-millimeter camera from about 150° west longitude to 60° east longitude. Sufficient detail was available to permit photographic reconstruction of the lunar surface.

c. Of 51 planned targets of opportunity using the 70-millimeter electric camera, time permitted photography of only 31. The targets were selected to enhance knowledge of specific features or to provide broad coverage of areas not adequately covered by Lunar Orbiter photographs.

d. Photography using the 16-millimeter data acquisition camera in conjunction with the sextant was performed over the proposed first lunar landing site and three control points. This photography indicated that landmark identification and tracking could readily be performed on lunar landing missions.

An analysis of the Apollo 8 photography is given in reference 3-56.

3.3.16 Lunar Multispectral Photography

The multispectral photography experiment was sucesssfully accomplished on the Apollo 12 mission. Its purpose was to obtain lunar vertical strip photographs in the blue, red, and infrared portions of the optical spectrum. Equipment consisted of an array of four 70-millimeter electric cameras with 80-millimeter lenses, three to satisfy experiment objectives and a fourth, with green filter, for operational purposes.

In addition to photographs of three planned targets of opportunity, continuous vertical strip photographs were obtained over the lunar surface from 118° east to 14° west longitude. The number of photographs obtained by each of the red-, green-, and blue-filtered cameras totaled 142, and the number of photographs taken by the infrared camera was 105. These photographs provided the first high-resolution (about 30 meters) look at subtle color variations on the lunar surface and the first study of color behavior at and near the point directly opposite the sun (zero phase). The experiment demonstrated the feasibility of multispectral photography and methods used to display color contrast (ref. 3-57).

3.3.17 Candidate Exploration Sites Photography

This detailed objective was accomplished on the Apollo 12 and Apollo 14 missions. Photographic tasks were intended to provide data for evaluating potential sites for follow-on lunar landing missions. Primary targets on Apollo 12 were three potential landing sites: Fra Mauro, Descartes, and Lalande. Although a malfunctioning film magazine prevented accomplishment of all desired photography, mandatory requirements were satisfied. These included the following: terminator-to-terminator stereoscopic coverage over three sites using the 70-millimeter electric camera with an 80-millimeter lens, and concurrent landmark tracking with the 16-millimeter data acquisition camera through the command and service module sextant; high-resolution photography of the three sites with the 70-millimeter electric camera with a 500-millimeter lens; and medium-resolution photography of other interesting areas such as Davy Rille with the 70-millimeter electric camera and 250-millimeter lens.

The primary photographic target for Apollo 14 was the area of Descartes Crater, the tentative landing site for Apollo 16. A main objective was to obtain high-resolution photographs of Descartes at both high and low altitudes using the lunar topographic camera. This objective was not completely satisfied because of improper operation of the lunar topographic camera. As a contingency measure, the 70-millimeter camera with a 500-millimeter lens was used to obtain high-resolution photographs of the Descartes area. Stereoscopic coverage of the area was also accomplished, although no camera shutter-open telemetry data were obtained because the S-band high-gain antenna did not operate properly.

3.3.18 Selenodetic Reference Point Update

The detailed objective of obtaining landmark tracking photographs for use in updating selenodetic reference points was successfully accomplished on the Apollo 12 and Apollo 14 missions. Lunar landmark tracking targets included the crater Lansberg A on the Apollo 12 mission and 11 landmarks on the Apollo 14 mission, ranging from 141° east longitude to 40° west longitude; major landmarks were the craters Daguerre 66, Dollond E, Mosting A, Enke E, and Ansgarius N. Landmark photographs were taken through the command and service module sextant using the 16-millimeter data acquisition camera; supporting photographs were taken with the 70-millimeter electric camera with an 80-millimeter lens.

3.3.19 Transearth Lunar Photography

Assigned to the Apollo 14 mission, the transearth lunar photography detailed objective was intended to provide photographic coverage of large areas on the far side and eastern limb of the moon. These photographs were to be obtained for use in extending selenodetic control and improving lunar maps. Both the 70-millimeter electric camera and the lunar topographic camera were scheduled for use; however, the lunar topographic camera malfunctioned in lunar orbit as discussed in section 3.3.17, and only the 70-millimeter camera was used. Both the 80- and 250-millimeter lenses were used with the 70-millimeter camera to photograph the visible disk of the moon after transearth injection. Features shown at high latitudes in these photographs were then related to features at lower latitudes which appeared in landmark tracking and stereoscopic photographs.

3.3.20 Service Module Orbital Photographic Tasks

Service module orbital photographic tasks were accomplished on the final three Apollo missions. The objectives of these tasks were to provide a data package consisting of tracking data, terrain photography, stellar photography, and altimetry. Tracking data essentially relate the spacecraft to an earth coordinate system. Terrain photography gives the relationship of the lunar surface to the spacecraft. In turn, the relationships between the lunar surface, lunar coordinate system, and earth coordinate system can be determined, yielding refined information about the lunar ephemeris with respect to the earth coordinate system. Terrain photography is also used in triangulation, an operation in which the geometry of all photographs taken on one or more missions can be integrated into a single unified coordinate system with a precision of about 20 meters in all three axes. Stellar photography, synchronized with metric photography of the lunar surface, relates the lunar and celestial coordinate systems and gives refined information about the lunar rotation rates, the orientation of its axis with respect to the celestial coordinate system, and its physical librations. Stellar photographs also permit the attitude of each terrain photograph to be determined independently so that lunar surface photographs can be related more precisely. Altimetry data, obtained from the command and service module in lunar orbit, gives a profile of the subtrack on the lunar surface as well as distance measurements of lunar surface features appearing in stereoscopic photographs; the altitude data allow photographs to be tied together rigidly.

Service module orbital photographic tasks involved operation of a panoramic camera, a mapping camera, and a laser altimeter. Instrument operation, anomalies, and the results of photographic tasks are summarized in the following paragraphs.

a. Panoramic camera photography. The panoramic camera was an adaptation of a military panoramic reconnaissance camera designed for high-altitude applications. From an altitude of 60 nautical miles, the camera covered a swath about 300 kilometers wide on the lunar surface, and provided photographs with a resolution of 1 to 2 meters. Panoramic photographs, in conjunction with 70-millimeter still camera photographs, were used for detailed photointerpretive studies. After rectification, panoramic photographs were also used for the production of large-scale topographic maps of landing sites and special features such as rilles, domes, and craters. Figures 3-9, 3-10 and 3-12 are examples of photographs taken with the panoramic camera.

The panoramic camera was flown successfully on the Apollo 15, 16, and 17 missions and produced outstanding photography of lunar features of very high resolution in both stereographic and monographic modes. On each of these missions, the lunar module could be seen in photographs of the landing areas and, in some instances, soil disturbances caused by the lunar roving vehicle and foot traffic could be seen. A total of 4697 photographs was recorded from these three missions. The areas of coverage are identified in references 3-58, 3-59, and 3-60.

The areas photographed on Apollo 15 included the Hadley Rille landing site, several areas being considered as the Apollo 17 landing site, the Apollo 15 lunar module ascent stage impact point, near-terminator areas, and other areas of general coverage. About 12 percent of the lunar surface was photographed. Anomalous operation of the velocity/altitude sensor was indicated on the first Apollo 15 panoramic camera pass on revolution 4 and on subsequent passes; however, good photographs were obtained over all critical areas and less than 1 percent of the total film exposed was seriously degraded by the sensor malfunction.

The velocity/altitude sensor measured the angular rate of travel of the spacecraft relative to the lunar surface. The sensor output was used to control the cycling rate of the camera, the forward motion compensation, and the exposure. The sensor normally operated in the range of 45 to 80 miles altitude. If, at any time, the indicated velocity/altitude was out of this range, the sensor automatically reset to the nominal value of 60 miles. The sensor operated properly for brief periods of time, but would drift off-scale high (saturate) and then reset to the nominal value corresponding to a 60-mile altitude. The results of tests, coupled with analyses of the basic sensor design, indicated that the problem was related to the optical signal-to-noise ratio. The remaining flight hardware was modified to improve this ratio.

Apollo 16 panoramic camera photography increased lunar surface coverage to about 15 percent, and included the Descartes landing area and prime targets at King Crater and in the Fra Mauro region. In addition, photographs of the lunar surface were obtained after transearth injection. During the mission, camera operation was stopped when an abnormal bus voltage condition was observed; subsequent inspection revealed that the condition was due to the spacecraft configuration

and not to a camera problem. Photography was rescheduled to obtain photographs lost while the camera was stopped. In addition to this anomaly, the camera exposure sensor consistently read lower light levels than were present. Postflight analysis indicated that frames taken about 25° away from the terminator were overexposed by 1-1/2 to 2 f-stops. To prevent recurrence of the anomaly on the Apollo 17 mission, sensor output voltage limits were added to preflight test procedures. A special process used to develop overexposed portions of film rolls compensated for the sensor problem. Task objectives were satisfied by the excellent quality photographs that were obtained.

Panoramic camera photographs obtained on the Apollo 17 mission increased total coverage of the lunar surface to approximately 20 percent. Multiple high-resolution photographs were obtained of the Taurus-Littrow landing site and of regions east and west of the areas photographed during the Apollo 15 and 16 missions. Photographs of the moon were also taken after transearth injection. The camera operated satisfactorily throughout the mission until the stereo drive motor failed just before the final photographic pass in lunar orbit; although some stereoscopic photography was lost and resulting monographic photography was degraded, mandatory photographic requirements were met.

b. Mapping camera photography. The mapping camera was designed to obtain high-quality metric photographs of the lunar surface from lunar orbit combined with time-correlated stellar photography for selenodetic/cartographic control. The camera received altitude information from a laser altimeter (discussed in the next subsection) once per frame in serial form. Timing signals were provided to the laser to permit the altitude to be obtained within 3 milliseconds of the center of exposure of the mapping camera.

Cartographic-quality photographs of all sunlit lunar surface areas overflown by the spacecraft as well as oblique photographs of large areas north and south of the groundtracks were obtained on the Apollo 15, 16, and 17 missions. Areas of coverage are identified in references 3-58, 3-59, and 3-60.

On the Apollo 15, 16, and 17 missions, the times required to extend and retract the mapping camera were considerably longer than those of preflight tests. Several corrective actions were taken, but the problem was not resolved. Although the mapping camera was left in the extended position for longer periods than planned, neither the quantity nor quality of photographic coverage was adversely affected.

Two other anomalies that occurred during the Apollo 16 mission concerned stellar camera glare shield jamming and metal chips in the film cassettes. During the extravehicular activity for film retrieval, the stellar camera lens glare shield was found in the extended position and was jammed against the service module handrail. Photographs taken from the lunar module indicated that the glare shield was properly retracted at rendezvous. As a result of this problem on the Apollo 16 mission, the Apollo 17 mapping camera drive rack was carefully realigned for proper pinion gear engagement when the camera assembly was fully deployed. The aforementioned metal chips were found during the reprocessing inspection of the Apollo 16 returned film. The chips were removed at the start of processing and caused no loss of data on the film.

Despite the problems described, photographic requirements were satisfied on all three missions.

c. Laser altimetry. The laser altimeter marked the first use of a solid-state laser in a spacecraft application. It was flown on each of the J-series missions: Apollo 15, Apollo 16, and Apollo 17.

The purposes of the laser altimeter operations were to provide a measurement of the distance from the spacecraft to the lunar surface in synchronization with each mapping camera exposure, and to provide topographic profiles for correlation with gravity anomalies obtained from tracking data.

During the first operating period on the Apollo 15 mission, the orbit was highly eccentric, causing the spacecraft to be below the laser altimeter minimum range of 40 nautical miles approximately half the time. Whenever the altitude was within the design range of the altimeter, valid data were obtained. In the second and third operating periods, the laser output began to degrade,

accompanied by a gradual decrease in the number of valid altitude measurements. A subsequent failure in the high-voltage section caused total loss of receiver sensitivity. No data were obtained during the last half of lunar orbital flight. The cause of the decreased laser output was thought to be contamination of the optical surfaces in the laser module. As a result, more stringent cleaning and assembly procedures were implemented, and a control circuit was added to sense the output and to increase the input voltage to the laser if the output decreased. The source of the high-voltage problem was verified by duplication in the laboratory. High-voltage breakdown in a vacuum relay was generating electromagnetic interference which was picked up by the receiver automatic gain control circuit. The automatic gain control circuit held the receiver at its minimum sensitivity, thereby causing loss of the return signal. The problem was corrected by removal of the relay from subsequent units.

On the Apollo 16 mission, the laser altimeter was operated for seven periods in accordance with the flight plan, as revised during the mission to accommodate a delay in the lunar module landing. The laser output again began to degrade during the second operating period but was compensated for by the control circuit which had been added after the Apollo 15 mission. During the seventh operating period, the control circuit had reached the limit of its compensation capability, and the percentage of valid data showed a marked decrease. Of the total quantity of data obtained on the illuminated side of the moon, approximately 70 percent was valid. Because reduced laser output had less effect on operation over nonilluminated areas, approximately 80 percent of the dark-side measurements was valid. The decrease in laser output during this mission was a repeat of that experienced during the Apollo 15 mission, except that the added control circuit did prolong the effective life of the altimeter. The cause of the problem was found to be contamination of the laser module optics by bearing lubricant and a decrease in flashlamp energy due to solarization of the quartz envelope. The bearings in the Q-switch rotor were changed to a type having the lubricant vacuum-impregnated into the ball retainer. The flashlamp envelope material was changed to a higher purity grade of quartz to eliminate solarization. In addition, the control circuit was modified so that its compensation was added in smaller increments.

The effectiveness of the changes implemented in the laser altimeter hardware as a result of the previously mentioned problems can be seen by performance of the instrument on the Apollo 17 mission. The number of operations that produced valid data exceeded 99 percent. No altimeter anomalies occurred during the Apollo 17 mission.

Apollo program laser altimeter data reveal that the mean radius of the moon is approximately 1738 kilometers. The data also show that the center of figure is offset from the center of mass by 2 to 4 kilometers along the earth-moon line. Additional details of the laser altimeter studies are given in references 3-61, 3-62 and 3-63.

3.3.21 Command Module Orbital Science Photography

The command module orbital science photography detailed objective was conducted during the Apollo 14 mission. The purpose was to obtain photographs of lunar surface areas of prime scientific interest and of specific segments of the lunar surface in earthshine and in low-level light near the terminators*.

The lunar topographic camera with an 18-inch lens was provided to obtain high-resolution (2 meters) stereoscopic photographs (with 60 percent overlap) of four lunar surface targets; the target having the highest priority was an area north of Descartes Crater, a candidate landing site for the Apollo 16 lunar module. Operation of the camera was noisy on the first of three scheduled passes, indicating a camera malfunction. An extensive postmission film development plan instituted for analysis of the two exposed 5-inch film rolls resulted in the recovery of 193 usable photographs. These photographs covered a segment of the central lunar highlands from the eastern rim of Theophilus Crater to a point northwest of Kant Crater. Two major units were included: Theophilus Crater ejecta and Kant Plateau materials.

High-resolution photographs of eight lunar surface targets were scheduled to be obtained with a 70-millimeter electric camera: three with a 500-millimeter lens, and five with a 250-millimeter lens. The 500-millimeter targets were photographed successfully, but only two of the 250-millimeter targets were obtained; photographs of the other three targets were deleted because of operational considerations. The 70-millimeter camera was also used to photograph a number of targets that had been scheduled to be photographed with the lunar topographic camera.

*Dividing line between illuminated and unilluminated lunar surface.

A sequence of photographs showing the lunar surface in earthshine and in low light levels near the terminator was accomplished successfully. A 70-millimeter electric camera with an 80-millimeter lens and a 16-millimeter data acquisition camera with an 18-millimeter lens were used. The photographic sequence started just before the command and service module crossed the sunrise terminator and continued past the terminator. Photographs covered the area located in the south-central portion of the Ocean of Storms in the vicinity of Kunowsky Crater and approximately 210 kilometers southeast of Kepler Crater. Details of the orbital science photography conducted on the Apollo 14 mission are given in reference 3-64.

3.3.22 Visual Observations from Lunar Orbit

Visual observations were an integral part of lunar exploration because the dynamic range and color sensitivity of the human eye cannot be matched by any one film type or sensing instrument and because, in special cases, on-the-scene interpretation of observed features or phenomena was needed. Visual observations were intended to complement photographic and other remotely sensed data obtained from lunar orbit. This detailed objective was successfully accomplished on the Apollo 15, 16, and 17 missions. The locations of many of the areas referred to in the following paragraphs may be found in figure 3-1.

The extraordinary success of the visual observations on the Apollo 15 mission proved the outstanding capabilities of man and his use in space flight. All 13 scheduled targets were observed and crew comments were relayed to earth. Targets were the craters Tsiolkovsky, Picard, Proclus, Cauchy, Littrow, Dawes, and Sulpicius Gallus; Hadley Rille; Imbrium Basin flows; the Harbinger Mountains; the Aristarchus Plateau; and areas to be observed after transearth injection. The following significant observations were made during this mission (ref. 3-65).

a. Fields of possible cinder cones were discovered on the southeast rim of the Sea of Serenity (Littrow Crater area) and on the southwest rim of the same mare basin (Sulpicius Gallus Crater area).

b. The lineated segment of the northwestern rim of Tsiolkovsky Crater on the lunar far side was interpreted as a landslide.

c. An excluded zone in the ray pattern around Proclus Crater on the west rim of the Sea of Crises was interpreted as caused by a fault system at the west rim of the crater.

d. Recognition of layering along crater walls (as opposed to terracing by faults and mass wasting by downward movement of materials along the walls) was achieved for the first time. This recognition gives a new dimension to thinking relative to the nature of the upper layers of the lunar crust.

Targets scheduled for visual observation on Apollo 16 were the farside highlands; the craters Mendeleev, King, Goddard, and Kapteyn; the Colombo highlands; the craters Isodorus-Capella; the Descartes landing site; and Alphonsus Crater. All but one of the targets were successfully observed; the Goddard target area was deleted because of time constraints. Items used to aid in observations were site graphic materials, a pair of 10-power binoculars, and a reference color wheel. The following significant observations were made (ref. 3-66).

a. The crew's first impression of the moon from lunar orbit was that of a brilliant, heavily battered, and uniformly colored body. Toward the end of lunar orbit, they felt that the detailed characteristics of units commonly mapped on the lunar near and far sides were surprisingly similar.

b. Fine scarps, generally irregular and somewhat subdued, were observed on the far side, but none was seen in the near-side highlands.

c. The Cayley Formation generally had the same appearance as large basin fill, as small patches in the bottom of the steep-sided craters, and as valley filling in the hummocky far-side highlands.

d. Mare surfaces provided the setting for the most obvious color contrasts.

e. Numerous terrace-like rims were detected along highland hills in the Sea of Clouds, the Known Sea, and the Ocean of Storms, these are interpreted as "high-water marks," representing the maximum depth of filling by mare lavas.

Nine lunar surface targets were scheduled for visual observation on Apollo 17. They were the craters Aitken, Arabia, and Copernicus; the Seas of Crises and Serenity; D-Caldera; the Taurus-Littrow landing site; Smyth's Sea; Reiner Gamma Crater; and Tsiolkovsky Crater. Four additional targets observed were Euler Hills, and the craters Gagarin, Korolev, and Pasteur. Crew aids were onboard graphic materials, a pair of 10-power binoculars, and a reference color wheel. All aids were useful except the color wheel which apparently did not include a color range comparable to actual lunar colors.

Because the Apollo 17 groundtracks repeated approximately 80 percent of the lunar surface area previously overflown on Apollo 15, much was already known about the features in question. For this reason, emphasis was placed on color tones of geologic units and details of small-scale features. Detailed descriptions of the observations are given in reference 3-67.

3.3.23 Gegenschein from Lunar Orbit

The Gegenschein from lunar orbit experiment was performed on the Apollo 14, 15 and 16 missions. Its purpose was to determine if a detectable accumulation of dust exists at the Moulton point of the sun-earth system and, thus, to establish whether sunlight reflected from dust particles at this location contributes significantly to the Gegenschein phenomenon. The 16-millimeter data acquisition camera with an 18-millimeter lens was used on the Apollo 14 mission, and a 35-millimeter camera with a 55-millimeter lens was used on the Apollo 15 and 16 missions.

On the Apollo 14 mission, three sets of photographs were required to meet experiment objectives. Each set consisted of two 20-second exposures and one 5-second exposure in quick succession. For the first set the camera was pointed near the antisolar direction; for the second set the camera was pointed midway between the antisolar direction and the computed direction of the Moulton point, as viewed from the moon; and for the last set the camera was pointed near the direction of the Moulton point. All requirements were satisfied. Both aiming and filming were excellent, and the experiment demonstrated that long exposures were practicable.

As planned for the Apollo 15 mission, photography of the Gegenschein and Moulton point was performed twice, and at least six exposures were obtained during each sequence. All photographs were unusable because of incorrect spacecraft attitudes resulting from errors incurred during analytical transformation of target coordinates to spacecraft attitudes. However, the operational performance of the 35-millimeter camera system, used for the first time on the Apollo 15 mission, demonstrated its feasibility for Gegenschein photography.

The Apollo 16 experiment objectives were the same as those for the Apollo 14 and 15 missions, and were accomplished satisfactorily. Ten desired exposures were obtained, five with 1-minute durations and five with 3-minute durations. Pointing accuracy and spacecraft stability were within specified limits. Photographic quality was good, and the solar radiation caused less degradation of the Apollo 16 film than that of the Apollo 14 and 15 film. Analysis of the photographs shows that the sky is definitely brighter in the antisolar direction than in the direction of the Moulton region and that much less than half the light seen on earth as the Gegenschein comes from particles lingering in the Moulton region.

3.3.24 Ultraviolet Photography - Earth and Moon

This photography experiment was conducted on the Apollo 15 and 16 missions. Its purpose was to obtain imagery of the earth and the moon at a series of wavelength intervals in the near-ultraviolet portion of the spectrum. Photographs of the earth were required to provide calibration data to support the study of planetary atmospheres by telescopic observations in the ultraviolet spectrum; photographs of the moon were needed to investigate short-wavelength radiation from the lunar surface. Accompanying color photographs were obtained to help interpret the ultraviolet appearance of other planets in our solar system, especially Mars and Venus.

Equipment for recording required experiment spectral data consisted of a 70-millimeter electric camera with a 105-millimeter ultraviolet transmitting lens, a spectroscopic film sensitive to the shorter wavelengths, a special command module window fitted with quartz panes to pass a large fraction of incident ultraviolet radiation, and four filters. One filter was centered at 3750 angstroms, a second at 3050 angstroms, and a third at 2600 angstroms; the fourth passed visible radiation above 4000 angstroms. The command module window was covered by a shield most of the time to limit periods of crew exposure to high ultraviolet radiation levels in direct sunlight or in light reflected from the lunar surface.

Apollo 15 photographic activity began in earth orbit when the first several sets of ultraviolet photographs were taken. During translunar coast, three sets of ultraviolet photographs recorded the spectral signature of the earth from distances of 50 000, 125 000, and 175 000 nautical miles. Lunar orbit activities included ultraviolet photography of the earth above the lunar horizon and two series of ultraviolet photographs that recorded the spectral data for lunar maria and highlands. Ultraviolet photographic activities were concluded during transearth coast by photographs of the earth taken shortly after the crew extravehicular activity to retrieve film cassettes from the service module cameras, and by two more sets of earth photographs obtained during the final 2 days before landing.

Apollo 16 ultraviolet photographs were scheduled to be obtained during translunar coast, in lunar orbit, and during transearth coast. Time constraints, unsatisfactory performance of the 2650-angstrom bandpass filter, and lunar image centering problems resulted in the loss of some data. However, 66 high-quality images of the earth and moon were recorded at varying distances. Four sets of ultraviolet photographs of the earth and one set of the moon were exposed at scheduled times during translunar coast. During lunar orbit, spectral data of highland terrain near the Descartes landing site were recorded. A sequence of ultraviolet photographs of the moon shortly after transearth injection and another of ultraviolet earth photographs taken a few hours before landing completed experiment activities.

3.3.25 Dim-Light Photography

Primary objectives of the dim-light photography detailed objective, accomplished on the Apollo 14 mission, were to obtain photographs of diffuse galactic light, zodiacal light, and lunar libration region L4; also, the dark side of the earth was photographed through the sextant. Many of these observations were of the nature of an operational test to determine the feasibility of obtaining photographs of astronomical phenomena from the command and service module using a 16-millimeter data acquisition camera. A total of 56 exposures were made: 13 of galactic light, 30 of zodiacal light, 4 of lunar libration region L4, and 9 of the dark side of the earth through the sextant.

Zodiacal light could be seen with the unaided eye on about 15 photographs; galactic light and lunar libration photographs, though faint, were usable. Earth dark-side photographs were unusable because scenes were obscured by scattered light from the sextant optics, from sunlit areas of the earth, and perhaps from portions of the docked lunar module during translunar coast.

3.3.26 Command Module Photographic Tasks

The command module photographic tasks were performed on the Apollo 15, 16, and 17 missions. The portions of this detailed objective that supported astronomy investigations involved photography of the solar corona, zodiacal light, lunar surface areas in earthshine and in low light levels near the terminator, galactic light, and lunar libration region L4. Also the dark side of the earth and selected star fields were photographed through the sextant. Specific tasks assigned and cameras used included the following.

Task	Cameras, mm
Observations of solar corona	70 and 16
Moon during eclipse by the earth	70 and 35
Star fields through the command module sextant	16
Lunar libration region L4	16 and 35
Zodiacal light	16 and 35
Specific segments of lunar surface:	
In earthshine	35
Near terminator	70
Galactic light	16 and 35
Dark side of the earth through command module sextant	16

Command module photographic tasks scheduled for the Apollo 15 mission were designed to continue and expand those accomplished on the Apollo 14 mission. Photographs of star fields through the sextant were obtained during translunar and transearth coast periods; solar corona calibration photographs and a sequence of photographs documenting the lunar eclipse were taken during transearth coast. All other photographic objectives were achieved in lunar orbit.

Objectives of the command module photographic tasks for the Apollo 16 mission were to obtain photographs of the diffuse galactic light of celestial subjects, the solar corona, the zodiacal light, and specific segments of the lunar surface in earthshine and in low light levels near the terminator. These objectives were a continuation of the diffuse galactic light photographic task accomplished on the Apollo 14 mission and the dim-light command module photographic tasks performed during the Apollo 15 mission. Primarily because of time constraints, photographic objectives were not fully satisfied: only two of the four scheduled solar corona photographic sequences were completed, and lunar earthshine photography was not accomplished, although some photographs were obtained over areas less desirable than those planned. Other requirements were satisfied by photographs taken of lunar surface areas in low light levels near the terminator and two 5-minute exposures of diffuse galactic light in the Gum Nebula.

Apollo 17 command module photographic task objectives, a repetition of those for the Apollo 15 and 16 missions, were to obtain photographs of the solar corona, zodiacal light, and specific segments of the lunar surface in earthshine and areas in low light levels near the terminator. The first of two planned solar corona photographic sequences was successfully accomplished, but the second was omitted because of an extended crew sleep period. Seven photographs provided data on the east limb of the sun; two coronal streamers are evident in photographs taken just before sunrise, one lying nearly along the ecliptic. Exposure durations were as planned, permitting good photometry using preflight calibrations.

Zodiacal light, extending eastward from the lunar-occulted sun, was recorded in three separate series of photographs. A red filter was used for the first series, a blue filter for the second series, and a polarizing filter for the third series. When corresponding red and blue images were compared, the inner zodiacal light within about 15° of the sun showed a stronger red component in and close to the ecliptic plane, whereas inner zodiacal light well out of the ecliptic plane and almost all of the outer zodiacal light produced a stronger blue component; although a similar visual comparison of equivalent polaroid frames did not show any obvious variation in features, excellent isophote maps can be made for the most sensitive comparison necessary in the future.

High-quality photographs of lunar surface targets in earthshine were obtained. These targets were the craters Eratosthenes, Copernicus, Reiner Gamma, Riccioli, and Orientale. Other crew-option targets that were photographed using blue, red, and polarization filters included Tsiolkovsky Crater, the Sea of Rains, and the Taurus-Littrow landing site. Photographs of lunar surface areas in low light levels near the terminator were of excellent quality, particularly those located in the near-side mare areas.

3.4 EARTH RESOURCES PHOTOGRAPHY

Earth resources photography included synoptic terrain photography and synoptic weather photography, performed on Apollo 7, and multispectral terrain photography, performed on Apollo 9. The purposes of these experiments were to obtain high-quality color, panchromatic, and multispectral photographs of selected land and ocean areas of the earth and of clouds and other weather phenomena. Data from these photographs supplemented existing earth resources data, thus enhancing meteorological and ecological knowledge.

Photographs for all experiments were obtained by using modified 70-millimeter electric cameras. For the multispectral terrain photography experiment, an array of four electric cameras was used with four film/filter combinations: Panatomic-X film with red and green filters, infrared black-and-white film with a red filter, and color infrared film with a Wratten 15 filter.

3.4.1 Synoptic Terrain Photography

More than 500 synoptic terrain photographs were obtained during the Apollo 7 mission. Of these, about 200 satisfied experiment objectives. Photographs obtained were used to support studies of the origin of the Carolina bays in the United States, wind erosion in desert regions, coastal morphology, and the origin of the African rift valley. Near-vertical, high-sun-angle photographs of Baja California, other parts of Mexico, and parts of the Middle East were useful for geologic studies. Photographs of New Orleans, Louisiana, and Houston, Texas, were generally better for geographic urban studies than those available from previous programs. Areas of oceanographic interest, particularly islands in the Pacific Ocean, were photographed for the first time. In addition, the first extensive photographic coverage of northern Chile, Australia, and other areas was obtained.

3.4.2 Synoptic Weather Photography

Of the approximately 500 synoptic weather photographs obtained during the Apollo 7 mission, 300 showed clouds and other items of meteorological interest, and 80 contained features of oceanographic interest. Categories considered worthy of additional interest included weather systems such as tropical storm; winds and their effects on clouds; ocean surfaces; underwater zones of Australian reefs, the Pacific Atolls, the Bahama Islands, and Cuba; landform effects; climatic zones; and hydrology. Of particular interest were photographs of Hurrican Gladys and Typhoon Gloria, photographed on October 17 and October 20, 1968, respectively.

3.4.3 Multispectral Terrain Photography

Photographic targets for the multispectral terrain photography experiment were primarily in the United States and Mexico. Coast-to-coast coverage of parts of the United States and parts of southern Mexico and Central America was accomplished; partial photographic sets were obtained of test areas specifically designated for oceanographic and meteorological studies. Typical sites were Phoenix and Yuma, Arizona; Houston, Texas; Los Angeles, California; and Mexico City, Mexico. Secondary targets were located in Africa. A total of 584 frames were exposed by all four cameras, yielding 127 complete photographic sets.

Except for some cloud cover, the quality of the multispectral terrain photographs ranged from very good to excellent. Photographic coverage of clouds and specific meteorological phenomena had greater value for meteorological application than photographs obtained during any previous manned orbital mission. Of the four film/filter configurations used, the color infrared

film/Wratten 15 filter combination provided the best photographic information and resolution, and rapid discrimination was possible between features such as water, types of vegetation, and rocks or soil. Of the three black-and-white film/filter combinations, Panatomic-X film/red filter produced the best tone differentiation, contrast, and resolution; infrared film/red filter provided the best discrimination between types of vegetation and provided the ability to reconstitute color imagery; and Panatomic-X film/green filter, the least effective of the four film/filter combinations, yielded a lower variation in shades of gray and less resolution than those obtained with the Panatomic-X film/red filter.

3.5 BIOMEDICAL EXPERIMENTS

Three inflight biology experiments were conducted during the Apollo series of space flights. Each study investigated the effects of space flight, including ambient radiation, on one or more species of living organisms. A brief and general description of each experiment with a synopsis of previously reported observations is included.

3.5.1 Microbial Response to Space Environment

The objectives of the microbial response to space environment experiment were twofold. The first objective was to establish a statistically valid relationship between space flight and the viability of several different microbial systems. A second, more extensive objective was to analyze accurately the effect of space flight conditions on the rate of mutations and developmental changes in different micro-organisms.

The experiment systems are summarized in table 3-VIII. In most cases, the studied phenomena represent well-known model systems that can be directly correlated with disease or other medically important conditions that could affect the health of future astronauts. Investigators were invited to study those phenomena within their area of expertise and to conduct critical investigations in their laboratories. This method allowed many individual studies to be conducted in a coordinated manner and permitted a variety of micro-organism species to be housed within a single piece of flight hardware.

Each investigator selected a species of micro-organism that was nonpathogenic to man (to avoid possible contamination of the crew), that was well characterized relative to the phenomenon to be studied, that was well suited to simple and rapid screening tests, and that was compatible with the unique environment of the flight hardware. Dose-response studies were made possible by providing a mechanism to expose test systems to the full light of space or to components of the solar ultraviolet spectrum at peak wavelengths of 254, 280, and 300 nanometers, over a range of energy values.

During the Apollo 16 transearth coast extravehicular activity, the experiment hardware was removed from the crew compartment and affixed to the distal end of the television boom, which was then attached to the handle of the opened hatch door (fig. 3-31). Following a small command module attitude adjustment, the experiment was opened to expose the test systems to the direct rays of the sun. After exactly 10 minutes, the device was closed, brought back into the command module, and subsequently returned to earth for analysis.

A summary of the preliminary results of each microbial system is presented in the following paragraphs.

Aeromonas proteolytica produces an endopeptidase that can cause intracutaneous hemorrhage and necrosis in laboratory animals and another factor that can hemolyze human erythrocytes. This microbe was retained in fluid suspension and was exposed to all wavelengths of ultraviolet irradiation. Comparisons of survivors recovered from the experimental and control units indicate no significant differences in viability. The more sensitive characteristics of endopeptidase and hemolysin production are still being investigated.

TABLE 3-VIII.- MICROBIAL RESPONSE TO SPACE ENVIRONMENT EXPERIMENT SYSTEM COMPONENTS

Phenomenon studied	Assay system	Micro-organism
Biological Components		
Lipolytic α toxin production Deforming β toxin production Fatal δ toxin production	Lytic zone on agar *Sarcina flava* and house fly Silk worm and crystal assay	*Bacillus thuringiensis*
Infectivity	Mouse	*Nematospiroides dubius*
Hemorrhagic factor production Hemolytic enzyme procuction	Guinea pig and hemoglobin Human erythrocytes	*Aeronmonas proteolytica*
Genome alteration	Spore production	*Bacillus subtilis* spores, strains HA 101 (59) and HA 101 (59) F
UV and vacuum sensitivity	Colony formation	*Bacillus subtilis* spores, strain 168
Bacteria phage infectivity	Host lysis	*Escherichia coli* (T-7 phage)
Cellulolytic activity	Cloth fibers	*Chaetomium globosum*
Animal tissue invasion	Human hair	*Trichophyton terrestre*
Drug sensitivity	Antibiotic sensitivity in agar	*Rhodotorula rubra* *Saccharomyces cerivisiae*
Dosimetry Components		
High-energy multi-charged particles	Passive nuclear track detectors	Lexan Cellulose nitrate Photographic emulsion Silver chloride
Ultraviolet light	Passive dosimeters	Potassium ferrioxalate actinometry Photographic emulsion
Penetration of galactic irradiation	Thermoluminescent dosimeters	Lithium fluoride

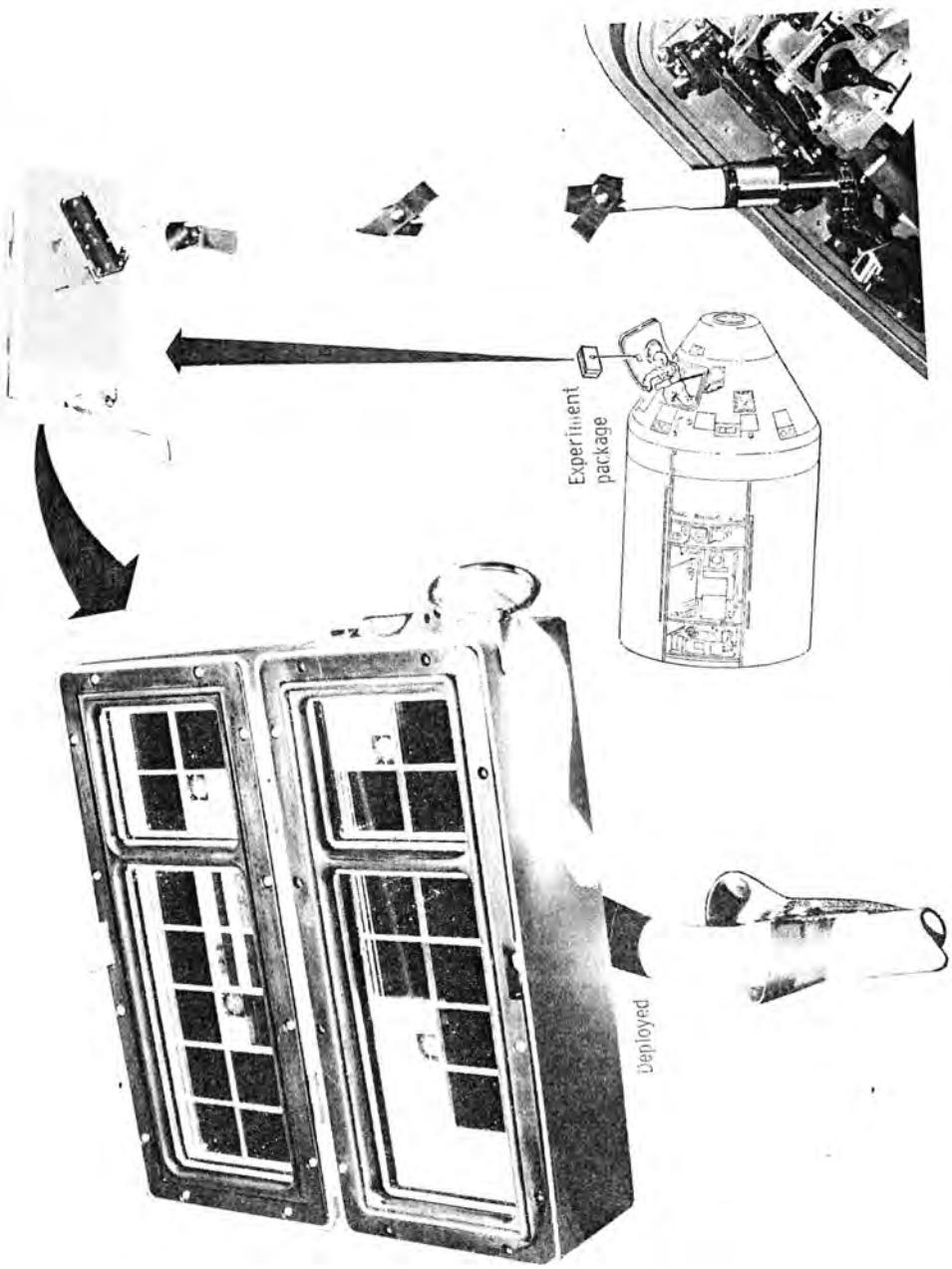

Figure 3-31. - Hardware for the microbial response in space environment experiment.

Two species of filamentous fungi, *Trichophyton terrestre* and *Chaetomium globosum*, were selected because these species are active against human hair and cloth fibers, respectively. The two species of yeasts, *Rhodotorula rubra* and *Saccharomyces cerevisiae*, were included because they may be used as biological indicators in several assay procedures. Detailed results of analyses have not yet been released.

Two different investigative groups evaluated different strains of *Bacillus subtilis*. Spores of *B. subtilis* strain 168 were exposed in monolayers to space vacuum and/or to ultraviolet irradiation at a peak wavelength of 254 nanometers. Detailed analyses of recoverable colony-forming units demonstrate that neither space vacuum nor ultraviolet irradiation in space nor a combination of these factors affected the survival of this strain in a manner discernible from the ground control and ground test subjects.

Spores of *B. subtilis* strains HA 101 (59) and HA 101 (59) F were exposed to the space flight environment in aqueous suspensions and in dry layers. Spores of these strains were selected because of their known stability in extreme environments. As with strain 168, comparisons of nonirradiated flight cells with ground controls as yet have failed to demonstrate any space-flight-mediated effect.

The species *Bacillus thuringiensis* var. *thuringiensis* was chosen for the experiment because it produces a lipolytic α toxin, a deforming β toxin, and a crystalline δ toxin, and because it has been widely used as a biological insecticide. As with the other bacilli, the space-flight conditions appear to have had no effect on cell viability as measured by surviving colony-forming units.

Survival studies of the T-7 bacteriophage of *Escherichia coli* were performed in an attempt to relate the present experiment to the space-flight-mediated effects reported by Russian scientists for *E. coli* phage specimens flown on numerous manned flights. Rather than the T-1 or K-12 (λ) phage commonly used on the Russian flights, the simpler and more stable T-7 phage was chosen for this study because this phage was expected to be more resistant to the rigors of space flight and thus would be a better ultraviolet test subject. Early calculations support this hypothesis because large losses in the flight subjects, as compared to the ground controls, are not indicated. Critical comparisons of flight and control test samples demonstrate no discernible space-flight-mediated antagonism or synergism.

The nematode *Nematospiroides dubius* was chosen for study because this complex multicellular organism has been successfully cultured in vitro from the egg to the third-stage infective larvae, is pathogenic to laboratory mice but not to humans, and is quite insensitive to the special holding conditions of the flight hardware. A comparison of nonirradiated flight and ground control subjects revealed no differences in survival, infectivity in mice, formation of adults, or subsequent egg productions. However, data analyses indicate that the space-flight environment (excluding ultraviolet irradiation and vacuum) profoundly affected the ability of the resulting eggs to develop to infective larvae.

Galactic irradiation measurements were conducted in response to current concern for the effect of high-energy multicharged particles on biological systems. Several systems including lithium fluoride, cellulose nitrate, Lexan, Ilford G5, and silver chloride crystals were used in the flight hardware and ground controls. The mean dose within the flight hardware was 0.48 ±0.02 rad with a range of 0.44 to 0.51 rad. This dose represents a total absorption of 48 ±2 ergs of ionizing energy per gram within the biological systems. Doses to the crewmen were slightly higher, ranging from 0.48 to 0.54 rad with a mean of 0.51 ±0.02 rad. Analyses of the Lexan and cellulose nitrate tracks and lithium fluoride values indicate that the microbial response hardware was better shielded during the flight than were either the Apollo light flash moving emulsion detector, the crew passive dosimeters, or the biostack experiment.

In conclusion, none of the available data indicate space-flight-mediated changes in cell viability or recovery. One significant observation is that *N. dubius* eggs produced after mice had been infected with space-flown *N. dubius* larvae demonstrated a significant decrease in hatchability when compared to identical ground controls. Except for the fact that the Apollo 16 flight larvae had been on board the command module, treatment of the flown larvae and ground control larvae was the same; neither had been exposed to ultraviolet irradiation.

3.5.2 Biostack Experiment

The biostack experiment studied the biologic effects of individual heavy nuclei of galactic cosmic radiation during space flight. A consortium of European scientists and engineers proposed and conducted the experiment. Although officially sponsored by the German Bundesministerium fur Bildung und Wissenschaft, the biostack was a representative segment of the scientific program of the Council of Europe designed to promote European research on the effects of high-energy/high-atomic-number particles of galactic cosmic radiation on a broad spectrum of biologic systems, from the molecular to the highly organized and developed forms of life. Two experiments were conducted - biostack I on Apollo 16 and biostack II on Apollo 17. The experiment approach was identical on both missions, and only a slight change in exposed biologic material was made between the two flights.

The objectives of the biostack experiment were achieved by using a hermetically sealed aluminum container (fig. 3-32) that contained a series of monolayers of biologic material sandwiched between several different types of detectors of galactic cosmic radiation particles. The biologic effects of high-energy particles under consideration included the following.

a. Physicochemical inactivation of molecular and cellular function

b. Radiation-induced mutations leading to genetic changes of biologic significance

c. Modification of the growth and development of tissues

d. Radiation-induced damage to nuclei and other subcellular functions

The biologically passive or dormant systems used in the biostack experiments were alternately stacked between physical detectors of high-energy/high-atomic-number particle tracks, which included nuclear emulsions (Ilford K2 and K5) and plastics (cellulose nitrate and polycarbonate), as well as lithium fluoride thermoluminescent (radiation) dosimeters located at the top and bottom of the biostack. A typical configuration of biologic layers and detectors is illustrated schematically in figure 3-33. This arrangement was used because the configuration permitted correlation of the incident high-energy/high-atomic-number particle with its interaction with the "hit" biologic material and the physicochemical characteristics and properties of the particle. This characterization of a specific particle identified with a specific biologic hit is critical in the evaluation of high-energy effects.

The following biologic system were included in biostack I on board Apollo 16.

a. Spores or inactive forms of the bacterium *Bacillus subtilis*

b. Dry seeds of *Arabidopsis thaliana*, commonly known as the European watercress

c. Radiculae or embryos of the bean *Vicia faba*

d. Encysted eggs of the brine shrimp *Artemia salina*

The systems in biostack II on board Apollo 17 included, once again, *Bacillus subtilis* spores and *Artemia salina* eggs. *Vicia faba* and *Arabidopsis thaliana* were deleted, and cysts of the protozoan *Colpoda cuculus*, eggs of the flour beetle *Tribolium confusum*, and eggs of the grasshopper *Carausius morosus* were added.

3.5.3 Biological Cosmic Radiation Experiment

The biological cosmic radiation experiment was a passive experiment intended to determine if heavy particles of galactic cosmic radiation have the capability to inactivate nondividing cells such as those in the brain and the retina of the eye. The experiment was conceived as a logical extension of earlier biological cosmic radiation studies that used balloon-borne animals. In this experiment, five *perognathus longimembris* (little pocket mice) were exposed to the galactic cosmic radiation encountered during the Apollo 17 lunar mission. This species was selected because the adult animal is small and these mice do not require water. A radiation dosimeter was implanted underneath the scalp of each animal to permit correlation of tissue lesions with the passage of radiation particles into the brain.

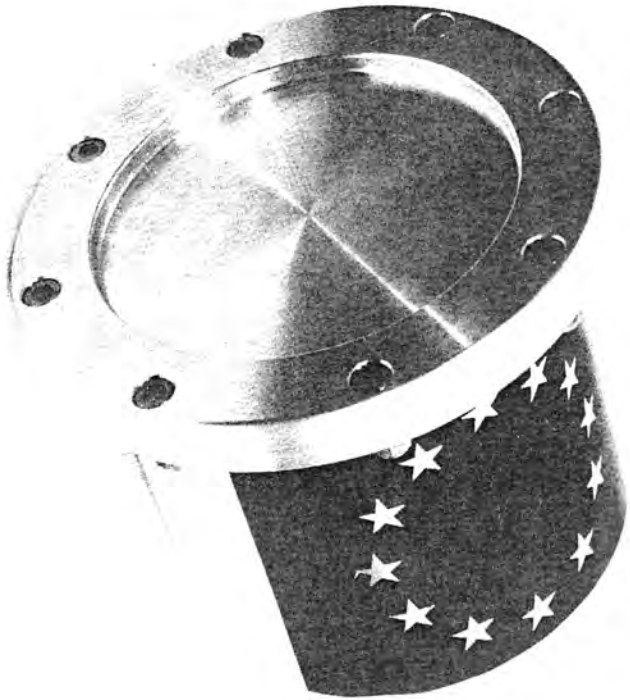

(a) Hermetically sealed.

(b) Monolayers of biologic materials and detectors of galactic cosmic radiation particles.

Figure 3-32. - The biostack.

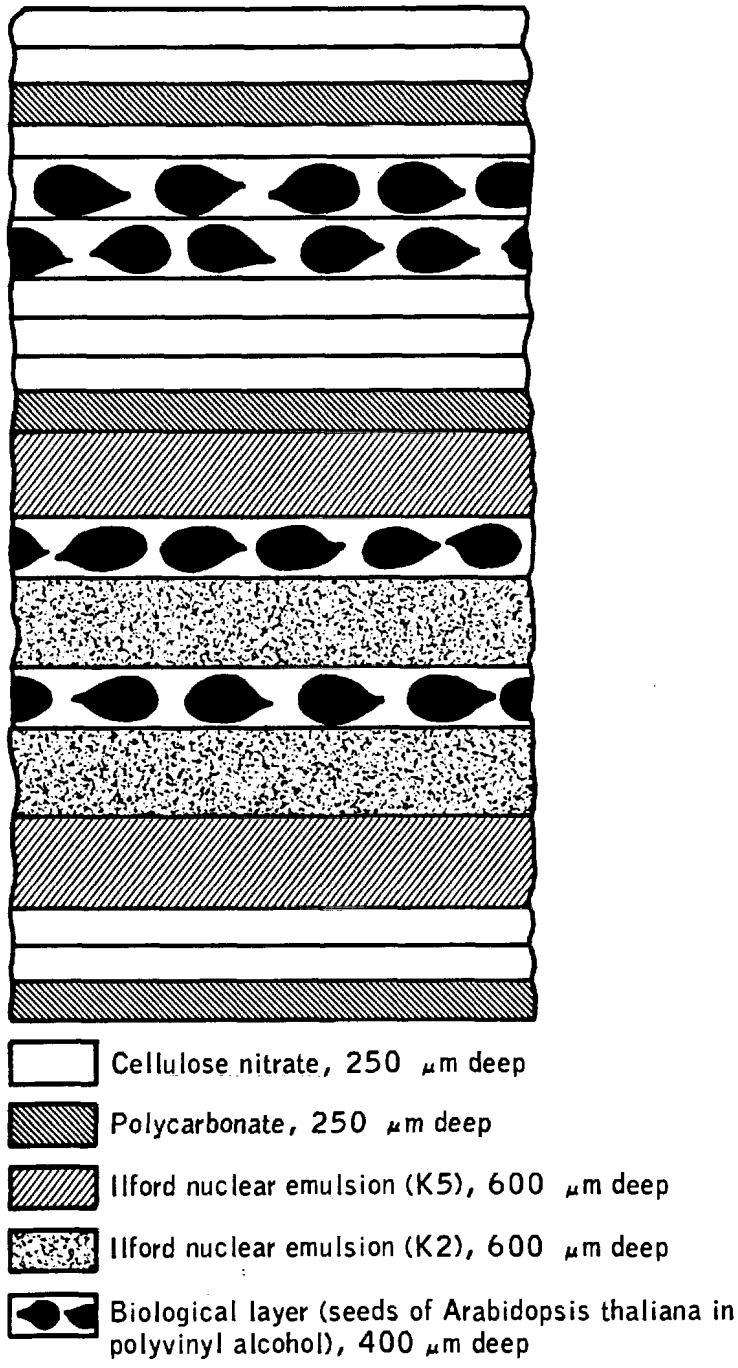

Figure 3-33.- Typical configuration of biologic layers and detectors in the biostack.

The hardware consisted of a hermetically sealed, cylindrical aluminum canister (approximately 13.5 inches long and 7 inches in diameter) that contained seven perforated, cylindrical metal tubes (fig. 3-34). Attached to one end of the canister were redundant pressure relief valves and two manually controlled purge valves. Six of the seven tubes were arranged around the inside wall of the canister. Five of these 1-inch-diameter aluminum tubes contained a mouse and its food supply. The sixth mouse tube was flown empty. The seventh tube, made of stainless steel, was centrally located in the six-tube circular arrangement. This center tube contained potassium superoxide granules for life support and operated by converting the carbon dioxide from the mice into oxygen. Two self-recording temperature sensors were located in two of the mouse tube end caps. A separate radiation dosimeter was located in the stowage locker adjacent to the experiment hardware.

The experiment was secured in the command module with its longitudinal axis perpendicular to the thrust axis during launch and recovery. The mice were loaded into the hardware approximately 4 days before the scheduled launch, and the experiment hardware was stowed in the command module approximately 36 hours before launch. The hardware was removed from the command module approximately 3 hours after landing and delivered to the Principal Investigator on American Samoa. The initial postflight processing of the flight mice was accomplished at a laboratory established for that purpose on American Samoa.

Four mice survived the Apollo 17 mission. The survivors appeared to be physiologically normal and displayed no behavioral manifestations indicative of any untoward effects of space flight. The death of the fifth mouse did not appear to be related to space flight stresses. The tissues of the mice are in pathological and histochemical analyses for any evidence of interaction between the tissues and heavy cosmic particles and subsequent biological damage. The subscalp dosimeters indicated penetration by a significant number of cosmic particles. Performance of the potassium superoxide granules in providing life support oxygen was considered to be normal.

3.6 INFLIGHT DEMONSTRATIONS

Inflight demonstrations were small carry-on experiments operated by several crews during translunar or transearth coast. The purpose of these experiments was to demonstrate the effects of near-zero gravity on various phenomena and processes. Demonstrations of fluid electrophoresis, liquid transfer, heat flow and convection, and composite casting were conducted on the Apollo 14 mission. In addition, another fluid electrophoresis demonstration was conducted on Apollo 16, and the heat flow and convection demonstration was repeated on Apollo 17. The composite casting demonstration was scheduled to be conducted again on the Apollo 15 mission but was canceled because of a hardware malfunction. Each demonstration is summarized briefly in the following subsections.

3.6.1 Fluid Electrophoresis

Electrophoresis is a separation technique used for classifying and analyzing delicate and complex mixtures of biological materials, for purifying biochemical products, and for medical diagnosis. Electrophoresis means "borne of electricity" and is the movement of charged particles in solution under the influence of an electric field. Most materials that can be divided into fine particles take on a charge when dispersed in an aqueous solution. The particles move through the fluid to the oppositely charged electrode at velocities dependent on their accumulated charge, size, and shape. After a period of time, particles separate into distinct zones, just as runners in a race spread out over the course. Each distinct zone of purified particles can then be extracted. Investigators believed that this separation process would be substantially improved in the near-zero-gravity space environment by reduction in the sedimentation and thermal convection mixing. The objective of this experiment, therefore, was to demonstrate electrophoresis separation in the space environment and, if proven effective, to show that small but significant quantities of biological materials such as vaccines, viral insecticides, and other valuable materials and products could be economically purified in space.

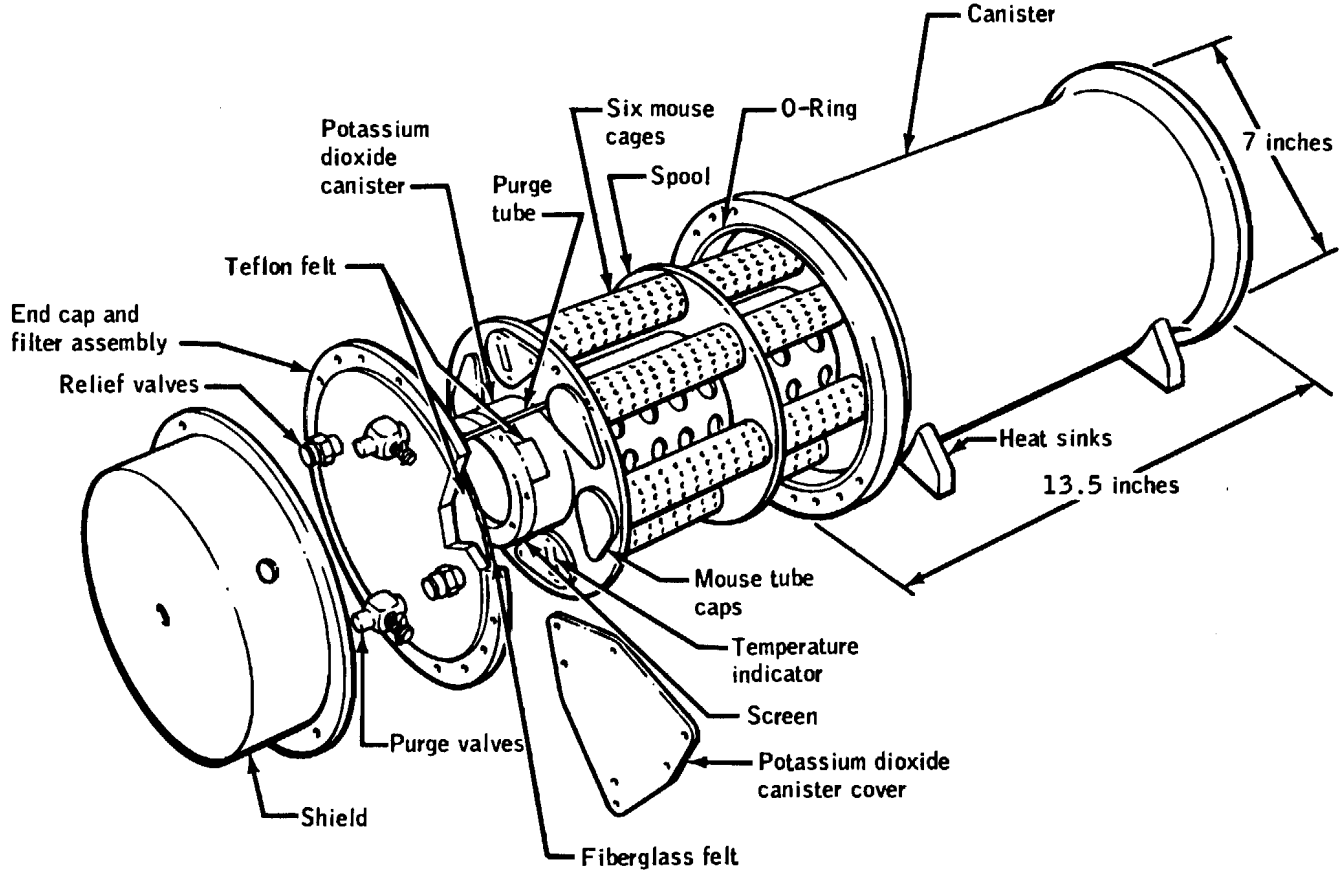

Figure 3-34.- Biological cosmic radiation (biocore) experiment package.

3.6.1.1 Apollo 14.- The Apollo 14 electrophoresis demonstration (ref. 3-68) was conceptualized and developed because of the great potential uses for this process. The experiment apparatus weighed about 5 pounds and was contained in a metal case (4 by 5 by 7 in.). The apparatus consisted of the electrical system, three electrophoresis cells, and a system to circulate the electrolyte through the cells. Each cell contained a different specimen: a red and a blue dye (for intense color and stability), hemoglobin (a high-molecular-weight biological material), and salmon sperm deoxyribonucleic acid (DNA) in an aqueous solution of boric acid.

The three experiments were run in parallel, and data were collected by photographing the action in the tubes sequentially with a 70-millimeter camera. The time required for the demonstration was 57 minutes. The results showed that the red and blue dyes separated as expected; but, because of apparatus and material problems, no action was seen in the hemoglobin or DNA tubes. (The hemoglobin and DNA may have been consumed during storage by bacterial action.) Nevertheless, much was learned about the technique and about the requirements for performing electrophoresis in space.

Conclusions drawn from analysis of the results are that (1) the resolution of the dye separation was much better in space than on earth, and (2) the shape and sharpness of the advancing boundary of separated materials was improved in space by the lack of sedimentation and convection currents, which were suppressed by the near-zero-gravity environment.

3.6.1.2 Apollo 16.- The Apollo 16 demonstration was designed to use the same basic operating elements used on the Apollo 14 mission. Although the case size and components were the same, the apparatus was heavier, weighing 7.5 pounds.

Two different particle sizes of polystyrene latex (0.2-micrometer and 0.8-micrometer diameter) were selected as the sample material to simulate the size and density of living cells. Three experiments were performed in parallel: cell 1 contained a mixture of the two sizes of latex particles, cell 2 contained only large particles, and cell 3 contained only small particles. The same experiment was done on earth to establish a control sample. Data were obtained from pictures taken automatically at 20-second intervals; the commentary transmitted by the flight crew provided additional information.

The flight pictures clearly showed the stability of the bands and the sharpness of the particle fronts during electrophoresis. By the time the samples were visible in the photographs, the front of each sample group had become pointed or bullet shaped. This shape was due to electro-osmosis of the buffer. Electro-osmosis is defined as the movement of liquid with respect to a fixed solid as a result of an applied electric field. Electro-osmosis was expected, and the apparatus was designed to minimize the effect. Large bubbles near the positive electrode distorted the electric field in this area, slowed the bands of particles in the area, and produced a corkscrew motion of the 0.8-micrometer particles in cells 1 and 2.

Interaction between identical and different particles was measured. The nose of the combined-particle band in cell 1 was composed primarily of 0.8-micrometer particles, and migration was slower than that of the 0.8-micrometer particles alone in cell 2. The leading band in both cells 1 and 2 was significantly more pointed than that of the 0.2-micrometer particles in cell 3. This phenomenon was attributed to interaction among the particles. Although a separation occurred, the 0.2-micrometer and 0.8-micrometer particles in cell 1 did not separate into distinct bands as expected.

The difficulties that limited the results of the Apollo 14 demonstration did not recur during the Apollo 16 demonstration, although the occurrence of electro-osmosis and formation of large bubbles near the positive electrode reduced the effectiveness of the demonstration. Future experiments will be aimed at solving these problems.

3.6.2 Liquid Transfer

One element of propellant management that will be necessary in future space operations will be transfer of liquid from a tanker vehicle to a receiver vehicle. The transfer of liquid from one container to another in a weightless environment was demonstrated by the Apollo 14 crew to determine the effectiveness of two configurations, each designed to achieve:

a. Gas-free outflow from the supply tank while obtaining a high total delivery efficiency.

b. Orderly inflow into the receiver tank with no liquid loss through the gas vent.

c. Location of the gas at the gas vent and the liquid at the drain/fill port.

To satisfy these conditions, the designs combined the desirable characteristics of existing baffle and screen concepts; one configuration was a standpipe-liner baffle design and the other was a curved-web baffle design. Reference 3-69 gives detailed descriptions of the two baffle configurations.

The demonstration apparatus consisted of a tank assembly unit, a hand-operated piston pump, and interconnecting flexible tubing. The tank assembly unit contained two pairs of model tanks. One pair had the internal surface-tension baffles that were to be demonstrated; the second pair had no baffle devices so that a comparison could be made. The model tanks were cylindrically shaped to simulate in two dimensions the three dimensional flow that would occur in a spherical tank. The tanks were 4 inches in diameter and the flat faces, separated by 0.25 inch, were of clear plastic for photographic purposes. Each tank contained two ports positioned 180° apart, representing drain/fill and vent lines. The drain/fill ports on each pair of tanks were connected by a transfer tube that contained a slide-action isolation valve. The vent ports had identical slide-action valves. A lighting frame containing six incandescent lamps and using spacecraft power provided the illumination necessary for photography. The external plastic surfaces that faced the lighting frame section were frosted to provide diffuse illumination, and all external plastic surfaces were covered with laminated safety glass and an overlay of thin fluoroplastic sheet to ensure maximum crew safety. The hand-operated piston pump was a screw-driven piston providing positive pressure on one side while creating suction on the other side. The pump could be operated in either direction. The tubing, sized for a friction fit over pump and tank port connections, could be easily switched to permit pumping between tanks in the baffled set or in the unbaffled set. The liquid used in the tanks was an inert chemical that satisfied the safety requirements for the spacecraft and simulated the static contact angle of most propellants on tank surfaces (nearly zero degrees). A small amount of dye was added to the liquid to improve the quality of the photographs.

The vent sides of a pair of tanks were connected to the pressure and suction sides of the pump, closing the system. The isolation valves on the vent ports were then opened, as well as the valve on the transfer tube interconnecting the drain/fill ports. Operation of the piston pump crank resulted in transfer of liquid from one tank to the other. On completion of a transfer operation, the crank was turned in the opposite direction to reverse the flow. One crewmember photographed the tanks either with the 16-millimeter sequence camera or the onboard television camera while the other operated the piston pump at a prescribed rate.

Several transfer operations were performed by the crew. The results of four of the operations are given in reference 3-69 as being representative of the results - three for the baffled tank system and one for the unbaffled tank system. The results are briefly summarized in the following paragraphs.

3.6.2.1 Unbaffled tanks.- In the weightless environment, the liquid/vapor interface for liquid transfer using unbaffled tanks is expected to be circular in shape, forming a gas bubble randomly located within the tank. The configuration at the start of liquid transfer consisted of a circular vapor bubble in the supply tank located such that a liquid layer covered both the drain and vent sides of the tank. The liquid filling was estimated to be 36 percent of the tank volume, with an additional 10 percent contained in the transfer tube connecting the two tanks. A gas bubble formed directly over the vent or pressurant inlet as the tank was pressurized to start the transfer.

During transfer, the liquid/vapor interface in the receiver tank was deformed because of the incoming liquid jet; however, the interface appeared stable. (The stability of the interface during liquid inflow is a function of the liquid jet velocity and, therefore, of the flow rate.)

Gas from the supply tank was ingested into the transfer tube when the liquid remaining was 24 percent of the tank volume. Continuation of the operation resulted in bubble entrainment and growth in the receiver tank. As expected, liquid eventually was ingested in the receiver tank vent.

3.6.2.2 Baffled tanks.- In the first of the three liquid-transfer operations performed with surface-tension baffled tanks, the curved-web-baffled tank was the supply tank and the standpipe-liner-baffled tank was the receiver tank. In the second test, the procedure was reversed. For these tests, the flow rate was the same order of magnitude as for transfer with the unbaffled tanks. The third transfer operation was performed at about four times the previous flow rate.

a. First operation: Liquid was transferred from the curved-web supply tank to the standpipe-liner receiver tank at an estimated flow rate of 0.83 cubic centimeter per second. As the transfer operation progressed, the liquid/vapor interface in the supply tank receded in an orderly fashion down to the point of incipient gas or vapor ingestion. During the same time, the receiver tank filled in an orderly manner with liquid filling the standpipe last. With the exception of a small amount of liquid in the capillary tube above the drain, nearly all the liquid in the supply tank was delivered to the receiver tank without gas ingestion from the supply tank and without liquid loss through the vent of the receiver tank, thereby successfully demonstrating the three design objectives.

b. Second operation: Liquid was transferred from the standpipe-liner supply tank to the curved-web receiver tank at an estimated flow rate of 0.67 cubic centimeter per second. As liquid drained from the supply tank, the standpipe emptied first, with the space between the standpipe and the liner draining next. The annular volume between the liner and the tank wall for this application is designed to remain full of liquid at the termination of transfer. This quantity represents the residual liquid inherent to this design. (Continuation of draining would result in an unpredictable vapor penetration anywhere along the wall liner, trapping liquid in the annulus.) Nearly all the supply tank liquid, with the exception of the liquid within the wall liner, was emptied without gas ingestion. During the filling of the receiver tank, the curved-web baffle controlled the interface position with no liquid loss through the gas vent. This transfer operation also demonstrated the orderly and efficient transfer of liquid in a weightless environment using surface-tension baffles.

c. Third operation: Liquid was transferred from the curved-web supply tank to the standpipe-liner receiver tank at a flow rate of 3.5 cubic centimeters per second. The receiver tank wall liner was full before initiation of flow. Again, during transfer, the interface in both tanks was stable and moved in an orderly fashion. At this higher flow rate, however, some differences occurred that are interesting to note. In the supply tank, the volume between the outermost web and the tank wall was the last to drain. These differences were attributed to variations in the dynamic pressure losses among the web channels. This conclusion indicates that the spacing of the webs and their perforations can be optimized by readjustment to provide uniform draining between webs. In this case, however, transfer was terminated when the interface for the inner webs reached the capillary tube over the drain, leaving a somewhat larger residual than for the transfer cases at lower flow rates. Similarly, the filling of the standpipe in the receiver tank lagged behind the filling of the rest of the tank, even more noticeably than for the first liquid transfer operation. However, unlike that transfer, the standpipe did not fill completely even at the end of transfer. This fact also indicates that the standpipe could be optimized by redesigning the spacing and perforations to improve the tank performance characteristics.

3.6.3 Heat Flow and Convection

A heat flow and convection demonstration was conducted on the Apollo 14 mission (ref. 3-70) during transearth flight and on the Apollo 17 mission (ref. 3-71) during translunar flight. For both missions, the demonstration unit contained three separate experiments. A flow pattern experiment was included to investigate convection caused by surface tension gradients resulting from heating a thin layer of liquid. A radial heating experiment was included to obtain information on heat flow in a confined gas under low-gravity conditions. A zone heating experiment was included to investigate heat transfer in confined liquids in a low-gravity environment.

3.6.3.1 Apollo 14 demonstrations.- The Apollo 14 demonstration apparatus consisted of a 9.0- by 9.0- by 3.8-inch box weighing 7 pounds. Four experiment configurations were mounted in the box - a flow pattern cell, a radial heating cell, and two zonal heating cells. Each cell contained a small electric heater powered by the spacecraft 28-volt-dc power source. The data were recorded by the 16-millimeter data acquisition camera attached to the unit and operating at a rate of one frame per second. Seven experiment operations were performed, each requiring 10 to 15 minutes.

a. Flow pattern cell: The flow pattern cell was designed to show the convective flow pattern induced in a thin layer of heavy oil (Krytox) by establishing a thermal gradient across the oil. The cell consisted of a shallow aluminum dish that was uniformly heated from the bottom. The oil was introduced from a reservoir, and a thermal gradient was established across the oil layer when the window to the cell was opened, with the heat being dissipated into the spacecraft atmosphere. Aluminum powder suspended in the oil allowed the flow patterns to be observed.

As a result of previous experiments that were conducted under one-g conditions, it was postulated that surface tension gradients (resulting from temperature gradients) are the predominant cause of cellular convection in thin layers of fluids (5-mm or less). The possibility remained, however, that gravity was an indispensible ingredient in all cellular convection, particularly as some second-order effect. The Apollo 14 experiment conclusively demonstrated that surface tension alone can generate cellular convection. The pattern of the convection was partially defined, but not in the desired constant depth configuration because wetting of the cell liner occurred.

b. Radial heating cell: The purpose of the radial heating experiment was to obtain information on the rate of temperature propagation in carbon dioxide gas while in the space environment. The cell was a cylindrical dish covered by a glass window. The glass was coated with a film containing a liquid crystal material that changes color when heated. The film was divided into quadrants, and different sectors were sensitive in different temperature ranges. The gas was heated by a small electrical stud heater mounted in the center of the cell. Changing color patterns indicated the temperature distribution as it developed, and the patterns were recorded by the camera. Two radial heating operations were performed, and the data quality was excellent.

Comparisons were made between flight data and analytical predictions based on the assumption that conduction and radiation were the only modes of heat transfer. It was concluded that convection was occurring in the radial cell, causing faster changes in temperature than can be attributed to thermal conduction and radiation. Although the convection could have been caused by low-gravity forces, it is more likely that some other unidentified non-gravity influence was responsible.

c. Zonal heating unit: The objective of the zonal heating experiment was to obtain data on the mode and magnitude of heat transfer in liquids subjected to zonal heating in a low-gravity environment. Heat transfer in configurations of the geometry of the zonal heating unit was of interest because this geometry is basic for many projected space manufacturing processes. The zonal heating cells consisted of two glass tubes with cylindrical heating elements surrounding the center portions of the tubes. One tube contained distilled water and the other, a 20-percent sugar solution. The sugar solution was used so that a comparison could be obtained between pure water and a fluid having a viscosity of approximately twice that of pure water. Temperature changes were sensed by liquid-crystal strips located along the center axes and along the walls of the tubes. Color patterns on the strips were monitored as heat flowed from the centrally heated zone toward the tube ends. Two zonal heating operations were performed and data quality appeared to be excellent.

3.6.3.2 Apollo 17 demonstration.- The Apollo 17 heat flow and convection demonstration was conducted as a follow-on to the Apollo 14 demonstration. The apparatus was similar to that used on Apollo 14, and the data were obtained in the same manner.

a. Flow pattern cell: Baffles were added around the periphery of the pan to maintain the liquid level at 2 and 4 millimeters in depth. Otherwise, the flow pattern experiment configuration was like that of the Apollo 14 unit. The experiment was operated twice, once with the 2-millimeter fluid depth and once with the 4-millimeter fluid depth. The fluid was contained by the baffles around the periphery and assumed a convex shape, similar to a lens.

The pattern of convection obtained for the 2-millimeter depth of oil was less orderly and less symmetrical than the patterns obtained with a ground-based unit, but they were more orderly and symmetrical than the pattern obtained on the Apollo 14 demonstration. The 4-millimeter-depth run showed more regular and larger cells. The results show that surface tension alone can cause a cellular convection flow of relatively high magnitude.

b. Radial heating and lineal heating units: The Apollo 17 radial and lineal (zonal) heating experiments were conducted to obtain additional information on heat flow and convection in confined gases and liquids. The experiment configurations were similar with the following major differences. In the radial heating experiment, the cell contained argon gas instead of carbon dioxide. In the lineal heating experiment, a single glass tube containing Krytox oil was used instead of two tubes containing water and a sugar-water solution. Also, the liquid in the Apollo 17 unit was heated by a disc heater at one end of the tube instead of a centrally located cylindrical heater. Temperature changes were monitored by liquid-crystal tapes immersed in the fluids.

3.6.3.3 Summary of interpretations.-

a. Flow pattern experiment:

1. The sizes of the observed surface tension-driven convection cells agree fairly well with those predicted by linear analysis of surface tension-driven cellular convection.

2. Convection occurred at lower temperature gradients in low-g than in one-g. Surface tension and gravity, therefore, apparently do not reinforce each other in a manner predicted by one analysis of cellular convection.

3. The flow pattern experiment data substantiate in principle the postulate that gravity modulates cellular convection onset.

4. The onset of a concentric side roll and center polygonal cells in the flow pattern experiment occurred at about the same time. The occurrence of a roll is contrary to expectations based on latest literature. The observed onset pattern tends to confirm an earlier view that rolls are sidewall effects and are not particularly characteristic of the driving mechanism.

b. Radial and lineal heating experiments: No significant convection was observed in the radial or lineal heating experiments. The data, however, validate the accuracy of the measuring technique and allow the conclusion that convection observed in the Apollo 14 radial and zone cells was probably caused by the heat flow and convection unit and spacecraft vibrations.

3.6.4 Composite Casting

Composite casting is defined as the casting of a material from a mixture of a liquid matrix and solid particles. A variation of composite casting is obtained when gas is added to form voids in the material to reduce weight and to control the material density. Another variation is obtained when normally immiscible (nonmixing) liquid materials such as oil and water are dispersed one in the other and solidified. On earth, materials of different specific gravities normally segregate from a mixture (e.g., sand and water) when at least one of the components of the mixture attains the liquid state. The purpose of the composite casting demonstration was to show that mixtures of materials having different specific gravities would remain stable (mixed) in the liquid state and during freezing in the low-gravity environment of space.

The composite casting demonstration was performed on the Apollo 14 mission during the translunar and transearth coast periods (ref. 3-72). The apparatus consisted of an electrical furnace, a heat sink device for cooling, and sealed metal capsules containing materials having a low melting point and dispersants (nonmelting particles). The furnace and heat sink package weighed slightly more than 2 pounds and measured 3.5 by 4.5 by 5.5 inches. The sample capsule weighed less than 0.5 pound and was 0.75 inch in diameter and 3.5 inches long. Procedures called for a crewman to insert each capsule into the furnace; to heat the capsule for a prescribed time; shake the materials in some cases in order to mix them; and to cool the furnace and capsule by placing them onto the heat sink.

Although 18 samples were provided, only 11 samples were processed because of time limitations. The evaluation of the 11 processed capsules consisted of comparing the space-processed (flight) samples with control samples processed on the ground under otherwise similar conditions. From the results, it was concluded that, in the low-gravity environment of space, the dispersions of particles, fibers, and gases in a liquid metal (matrix) were maintained during solidification.

The demonstration showed qualitative results in a very limited range of materials and under processing conditions that were not instrumented or closely controlled. Even so, the demonstrations were encouraging in that unique material structures were produced which provide a preliminary basis for processing materials and products in space. New problems were raised which can be solved by future ground and flight experiments. It is now evident that several factors must be considered for process and experiment design. These factors include the control of heating and cooling in low gravity when contact with heaters and heat sinks may be intermittent, control of nucleation and mixing, and control of gases for distribution in the melt or for removal from the melt.

3.7 REFERENCES

3-1. Brett, R.: Lunar Science. Essays in Physics, vol. 5, Academic Press, 1973, pp. 1-35.

3-2. Marvin, U. B.: The Moon After Apollo. Technology Review, vol. 75, no. 8, 1973, pp. 13-23.

3-3. Hinners, N. W.: The New Moon: A View. Revs. Geophys. and Space Phys., vol. 9, no. 3, 1971, pp. 447-522.

3-4. Milton, D. J.: Geologic Map of Theophilus Quadrangle of the Moon: Geologic Atlas of the Moon, Scale 1:1 000 000. U.S.G.S. Map I-546 (LAC 78), 1968.

3-5. Muller, P. M.; Sjogren, W. L.: Mascons; Lunar Mass Concentrations. Science, vol. 161, 1969, pp. 680-684.

3-6. Shoemaker, E. M.; Bailey, N. G.; Batson, R. M.; Dahlem, D. H.; et al.: Geologic Setting of the Lunar Samples Returned by the Apollo 11 mission. Sec. 3 of the Apollo 11 Preliminary Science Report, NASA SP-214, 1969.

3-7. Lunar Sample Analysis Planning Team: Summary of Apollo 11 Lunar Science Conference. Science, vol. 167, no. 3918, 1970, pp. 449-451.

3-8. Lunar Sample Preliminary Examination Team: Preliminary Examination of Lunar Samples From Apollo 12. Science, vol. 167, no. 3923, 1970, pp. 1325-1339.

3-9. Chapman, P. K.; Calio, A. J.; Simmons, M. G.: Summary of Scientific Results. Apollo 14 Preliminary Science Report, NASA SP-272, 1971.

3-10. Lunar Sample Analysis Planning Team: Third Lunar Science Conference. Science, vol. 176, no. 4038, 1972, pp. 975-981.

3-11. Muehlberger, W. R.; Batson, R. M.; Boudette, E. L.; Duke, C. M.; et al.: Preliminary Geologic Investigation of the Apollo 16 Landing Site. Sec. 6 of the Apollo 16 Preliminary Science Report, NASA SP-315, 1972.

3-12. Muehlberger, W. R.; Batson, R. M.; Cernan, E. A.; Freeman, V. L.; et al.: Preliminary Geologic Investigation of the Apollo 17 Landing Site. Sec. 6 of the Apollo 17 Preliminary Science Report, NASA SP-330, 1973.

3-13. Latham, G. V.; Ewing, M.; Press, F.; Dorman, J.; et al.: Passive Seismic Experiment. Sec. 11 of the Apollo 17 Preliminary Science Report. NASA SP-330, 1973.

3-14. Kovach, R. L.; Watkins, J. S.; and Landers, T.: Active Seismic Experiment. Sec. 7 of the Apollo 14 Preliminary Science Report. NASA SP-272, 1971.

3-15. Kovach, R. L.; Watkins, J. S.; and Talwani, P.: Lunar Seismic Profiling Experiment. Sec. 10 of the Apollo 17 Preliminary Science Report. NASA SP-330, 1973.

3-16. Dyal, P.; Parkin, C. W.; and Sonnett, C. P.: Lunar Surface Magnetometer Experiment. Sec. 4 of the Apollo 12 Preliminary Science Report, NASA SP-235, 1970.

3-17. Dyal, P.; Parkin, C. W.; and Sonnett, C. P.: Lunar Surface Magnetometer Experiment. Sec. 9 of the Apollo 15 Preliminary Science Report, NASA SP-289, 1972.

3-18. Dyal, P.; Parkin, C. W.; Colburn, D. S.; and Schubert, G.: Lunar Surface Magnetometer Experiment. Sec. 11 of the Apollo 16 Preliminary Science Report, NASA SP-315, 1972.

3-19. Dyal, P.; Parkin, C. W.; Sonnett, C. P.; DuBois, R. L.; and Simmons, G.: Lunar Portable Magnetometer Experiment. Sec. 13 of the Apollo 14 Preliminary Science Report, NASA SP-272, 1971.

3-20. Langseth, M. G.; Keihm, S. J.; and Chute, J. L., Jr.: Heat Flow Experiment. Sec. 9 of the Apollo 17 Preliminary Science Report, NASA SP-330, 1973.

3-21. Giganti, J. J.; Larson, J. V.; Richard, J. P.; and Weber, J.: Lunar Surface Gravimeter Experiment. Sec. 12 of the Apollo 17 Preliminary Science Report, NASA SP-330, 1973.

3-22. Talwani, M.; Thompson, G., Dent, B.; Kahle, H.; and Buck, S.: Traverse Gravimeter Experiment. Sec. 13 of the Apollo 17 Preliminary Science Report, NASA SP-330, 1973.

3-23. Simmons, G.; Strangway, D.; Annan, P.; Baker, R; et al.: Surface Electrical Properties Experiment. Sec. 15 of the Apollo 17 Preliminary Science Report, NASA SP-330, 1973.

3-24. Woolum, D.; Burnett, D. S.; and Bauman, C. A.: Lunar Neutron Probe Experiment. Sec. 18 of the Apollo 17 Preliminary Science Report, NASA SP-330, 1973.

3-25. Faller, J. E.: Laser Ranging Retro-Reflector Experiment Final Report. Contract NAS 9-11025, September, 1973.

3-26. O'Brian, B. J.; and Reasoner, D. L.: Charged-Particle Lunar Environment Experiment. Sec. 10 of the Apollo 14 Preliminary Science Report, NASA SP-272, 1971.

3-27. Snyder, C. W.; Clay, D. R.; and Neugebauer, M.: The Solar Wind Spectrometer Experiment. Sec. 5 of the Apollo 12 Preliminary Science Report, NASA SP-235, 1970.

3-28. Geiss, J.; Buehler, F.; Cerutti, H.; Eberhardt, P.; and Filleux, Ch.: Solar Wind Composition Experiment. Sec. 14 of the Apollo 16 Preliminary Science Report, NASA SP-315, 1972.

3-29. Eberhardt, P.; Geiss, J.; Graf, H.; Grogler, N.; et al.: Trapped Solar Wind Gases, Exposure Age and K/Ar Age in Apollo 11 Lunar Fine Material. Proceedings of the Apollo 11 Lunar Science Conference, supp. 1, vol. 2, Pergamon Press (New York), 1970, pp. 1037-1070.

3-30. Eberhardt, P.; Geiss, J.; Graf, H.; Grogler, N.; et al.: Trapped Solar Wind Noble Gases in Apollo 12 Lunar Fines 12001 and Apollo 11 Breccia 10046. Proceedings of the Third Lunar Science Conference, vol. II, MIT Press (Cambridge), 1972, pp. 1821-1856.

3-31. Hills, H. K.; Meister, J. C.; Vondrock, R. R.; and Freeman, J. W., Jr.: Suprathermal Ion Detector Experiment. Sec. 12 of the Apollo 15 Preliminary Science Report, NASA SP-289, 1972.

3-32. Freeman, J. W.; Hills, H. K.; and Vondrock, R. R.: Water Vapor, Whence Comest Thou? Proc. Third Lunar Science Conf., Geochim. Cosmochim. Acta, 1972, pp. 2217-2230.

3-33. Fleischer, R. L.; Price, P. B.; Burnett, D.; et al.: Cosmic Ray Experiment. Sec. 15 of the Apollo 16 Preliminary Science Report, NASA SP-315, 1972.

3-34. Berg, O. E.; Richardson, F. F.; and Burton, H.: Lunar Ejecta and Meteorites Experiment. Sec. 16 of the Apollo 17 Preliminary Science Report, NASA SP-330, 1973.

3-35. Johnson, F. S.; Carroll, J. J.; and Evans, D. E.: Lunar Atmosphere Measurements. Proceedings of the Third Lunar Science Conference, vol. 3, MIT Press (Cambridge), 1972, pp. 2205-2216.

3-36. Hoffman, J. H.; Hodges, R. R., Jr.; Johnson, F. S.; and Evans, D. E.: Lunar Atmospheric Composition Experiment. Sec. 17 of the Apollo 17 Preliminary Science Report, NASA SP-330, 1973.

3-37. Carruthers, G. R.; and Page, T.: Far UV Camera/Spectrograph. Sec. 13 of the Apollo 16 Preliminary Science Report, NASA SP-315, 1972.

3-38. Howard, H. T.; and Tyler, G. L.: Bistatic Radar Investigation. Sec. 25 of the Apollo 16 Preliminary Science Report, NASA SP-315, 1972.

3-39. Sjogren, W. L.; Muller, P. M.; and Wollenhaupt, W. R.: S-Band Transponder Experiment. Sec. 24 of the Apollo 16 Preliminary Science Report, NASA SP-315, 1972.

3-40. Sjogren, W. L.; Wollenhaupt, W. R.; and Wimberly, R. N.: S-Band Transponder Experiment. Sec. 14 of the Apollo 17 Preliminary Science Report, NASA SP-330, 1973.

3-41. Low, F. J.; and Mendell, W. W.: Infrared Scanning Radiometer. Sec. 24 of the Apollo 17 Preliminary Science Report, NASA SP-330, 1973.

3-42. Phillips, R. J.; Adams, G. F.; Brown, W. E., Jr.; Eggleton, R. E.; et al.: Apollo Lunar Sounder Experiment. Sec. 22 of the Apollo 17 Preliminary Science Report, NASA SP-330, 1973.

3-43. Anderson, K. A.; Chase, L. M.; Lin, R. P.; McCoy, J. E.; and McGuire, R. E.: Subsatellite Measurements of Plasmas and Solar Particles. Sec. 21 of the Apollo 15 Preliminary Science Report, NASA SP-289, 1972.

3-44. Anderson, K. A.; Chase, L. M.; Lin, R. P.; McCoy, J. E.; and McGuire, R. E.: Subsatellite Measurements of Plasma and Energetic Particles. Sec. 22 of the Apollo 16 Preliminary Science Report,NASA SP-315, 1972.

3-45. Coleman, P. J., Jr.,; Schubert, G.; Russell, C. T.; Sharp, L. R.: The Particles and Fields Subsatellite Magnetometer Experiment. Sec. 22 of the Apollo 15 Preliminary Science Report, NASA SP-289, 1972.

3-46. Coleman, P. J., Jr.; Lichtenstein, B. R.; Russell, C. T.; Schubert, G.; and Sharp, L. R.: The Particles and Fields Subsatellite Magnetometer Experiment. Sec. 23 of the Apollo 16 Preliminary Science Report, NASA SP-315, 1972.

3-47. Cour-Palais, B. G.; Brown, M. L.; and McKay, D. S.: Apollo Window Meteoroid Experiment. Sec. 26 of the Apollo 16 Preliminary Science Report, NASA SP-315, 1972.

3-48. Arnold, J. R.; Peterson, L. E.; Metzger, A. E.; and Trombka, J. I.: Gamma-Ray Spectrometer Experiment. Sec. 16 of the Apollo 15 Preliminary Science Report, NASA SP-289, 1972.

3-49. Arnold, J. R.; Metzger, A. E.; Peterson, L. E.; Reedy, R. C.; and Trombka, J. I.: Gamma-Ray Spectrometer Experiment. Sec. 18 of the Apollo 16 Preliminary Science Report, NASA SP-315, 1972.

3-50. Adler, I.; Trombka, J.; Gerard, J.; Schmodebeck, R.; et al.: X-Ray Fluorescence Experiment. Sec. 17 of the Apollo 15 Preliminary Science Report, NASA SP-289, 1972.

3-51. Adler, I.; Trombka, J.; Gerard, J.; Lowman, P.; et al.: X-Ray Fluorescence Experiment. Sec. 19 of the Apollo 16 Preliminary Science Report, NASA SP-315, 1972.

3-52. Gorenstein, P.; and Bjorkholm, P.: Alpha-Particle Spectrometer Experiment. Sec. 20 of the Apollo 16 Preliminary Science Report, NASA SP-315, 1972.

3-53. Hoffman, J. H.; Hodges, R. R.; and Evans, D. E.: Lunar Orbital Mass Spectrometer Experiment. Sec. 19 of the Apollo 15 Preliminary Science Report, NASA SP-289, 1972.

3-54. Hodges, R. R.; Hoffman, J. H.; and Evans, D. E.: Lunar Orbital Mass Spectrometer Experiment. Sec. 21 of the Apollo 16 Preliminary Science Report, NASA SP-315, 1972.

3-55. Fastie, W. G.; Feldman, P. D.; Henry, R. C.; Moos, H. W.; Barth, C. A.; et al.: Ultraviolet Spectrometer Experiment. Sec. 23 of the Apollo 17 Preliminary Science Report, NASA SP-330, 1973.

3-56. Analysis of Apollo 8 Photography and Visual Observations. Compiled by Johnson Space Center. NASA SP-201, 1969.

3-57. Goetz, A. F. H.; Billingsley, F. C.; Yost, E.; and McCord, T. B.: Apollo 12 Multispectral Photography Experiment. Sec. 9 of the Apollo 12 Preliminary Science Report, NASA SP-235, 1970.

3-58. Apollo 15 Mission Report. NASA Johnson Space Center Report MSC-05161, Dec. 1971.

3-59. Apollo 16 Mission Report. NASA Johnson Space Center Report MSC-07230, Aug. 1972.

3-60. Apollo 17 Mission Report. NASA Johnson Space Center Report JSC-07904, Mar. 1973.

3-61. Roberson, F. I.; and Kaula, W. M.: Apollo 15 Laser Altimeter. Sec. 25, Part D, Apollo 15 Preliminary Science Report, NASA SP-289, 1972.

3-62. Wollenhaupt, W. R.; and Sjogren, W. L.: Apollo 16 Laser Altimeter. Sec. 30, Part A, Apollo 16 Preliminary Science Report, NASA SP-315, 1972.

3-63. Wollenhaupt, W. R.; Sjogren, W. L.; Lingenfelter, R. E.; Schubert, G.; and Kaula, W. M.: Apollo 17 Laser Altimeter. Sec. 33, Part E, Apollo 17 Preliminary Science Report, NASA SP-330, 1973.

3-64. El-Baz, F.; Scott, D. H.; Milton, D. J.; Hodges, C. A.; Pohn, H. A.; Head, J. W.; et al.: Orbital Science Photography. Sec. 18 of the Apollo 14 Preliminary Science Report, NASA SP-272, 1971.

3-65. El-Baz, F.; and Worden, A. M.: Visual Observations from Lunar Orbit. Sec 25, Part A, Apollo 15 Preliminary Science Report, NASA SP-289, 1972.

3-66. Mattingly, T. K.; El-Baz, F.; and Laidley, R. A.: Observations and Impressions from Lunar Orbit. Sec. 28 of the Apollo 16 Preliminary Science Report, NASA SP-315, 1972.

3-67. Evans, R. E.; and El-Baz, F.: Geological Observations from Lunar Orbit. Sec. 28 of the Apollo 17 Preliminary Science Report, NASA SP-330, 1973.

3-68. McKannan, E. C.; Krupnick, A. C.; Griffin, R. N.; and McCreight, L. R.: Electrophoresis Separation in Space - Apollo 14. NASA TM X-64611, 1971.

3-69. Abdalla, K. L.; Otto, E. W.; Sumons, E. P.; and Petrash, D. A.: Liquid Transfer Demonstration On Board Apollo 14 During Transearth Coast. NASA TM X-2410, 1971.

3-70. Bannister, T. C.: Heat Flow and Convection Demonstration, Apollo 14, Summary Report. NASA Marshall Space Flight Center Report S&E-SSL-TR-71-1, 1971.

3-71. Bannister, T. C.; Grodzka, P. G.; Spradley, L. W.; Bourgeois, S. V; Heddon, R. O.; and Facemire, B. R.: Heat Flow and Convection Experiments. NASA TM X-64772, 1973.

3-72. Yates, I. C., Jr.: Apollo 14 Composite Casting Demonstration Final Report. NASA TM X-64641, 1971.

4.0 VEHICLE DEVELOPMENT AND PERFORMANCE

The first announcement of the Apollo program and its objectives was made in 1960. At that time, two techniques, direct ascent and earth-orbit rendezvous, were being considered for achieving a manned lunar landing. A third technique, lunar orbit rendezvous, was later determined to be more feasible and was eventually adopted in July 1962. Before this decision had been made, however, a preliminary program for manned lunar landings was formulated. Sufficient broadly applicable launch vehicle and spacecraft design requirements were identified in the preliminary studies to permit hardware development to proceed. Consequently, the basic Apollo spacecraft contract for the command and service module was awarded in 1961, and development of a large launch vehicle, which had begun in 1958, was changed and expanded to meet the goal of landing on the moon. The contract for the lunar module was awarded in November 1962.

The following discussion is divided into ten subsections. The first covers the design, development, and testing of the three series of Saturn launch vehicles used in the Apollo program. The second covers the Little Joe II test program. The remaining subsections contain discussions of the development and performance of the spacecraft and their major systems.

4.1 SATURN LAUNCH VEHICLES

4.1.1 Introduction

The Saturn family of large launch vehicles consisted of the Saturn I, Saturn IB, and Saturn V (fig. 4-1). Each of these played an important role in the Apollo program. Saturn I, the earliest of the vehicles, was used to test the structural integrity of the Apollo command module and the ability of its heat shield to withstand the temperatures generated on entry into the earth's atmosphere. The Saturn IB launch vehicle was used to launch the Apollo command and service module and the lunar module into orbit about the earth for testing in the space environment. The Saturn IB also launched the first manned Apollo spacecraft into orbit to check out both crew and spacecraft in space. When the Apollo program became operational, the Saturn V was used to launch the spacecraft into a translunar trajectory. The operational-payload configuration is shown in figure 4-2.

As early as April 1957, a team of engineers at the U.S. Army Ballistic Missile Agency, under the direction of Dr. Wernher von Braun, began studies of a large launch vehicle that could place 20 000- to 40 000-pound satellites into orbit about the earth or send 6000- to 12 000-pound payloads on escape missions from earth. In December 1957, this team proposed to the Department of Defense a large rocket with a thrust of 1.5 million pounds. A research program for such a vehicle was approved by the Advanced Research Projects Agency on August 15, 1958. The vehicle was originally named Juno 5, but the name was officially changed to Saturn on February 3, 1959. This Saturn became the first stage of the Saturn I and the forerunner of the first stage of the Saturn IB.

On July 1, 1960, the team developing the Saturn was transferred by President Eisenhower from the U.S. Army to the newly established National Aeronautics and Space Administration. Thus was formed the George C. Marshall Space Flight Center. While developing the Saturn I, the new center also began looking toward even larger launch vehicles in the summer of 1961. On January 25, 1962, the Saturn V was authorized as the launch vehicle for the Apollo program.

4.1.2 Saturn I

The Saturn I was a liquid-propellant, two-stage rocket. The first stage (S-I) consisted of a cluster of nine propellant tanks and eight H-1 engines, each producing 165 000 pounds of thrust. Using liquid oxygen and RP-1 (kerosene), the stage produced 1 320 000 pounds of thrust initially. Later, when the H-1 engine was uprated in performance to 188 000 pounds, the first stage had a thrust of 1 504 000 pounds. The second stage (S-IV) used liquid oxygen and liquid hydrogen in six RL-10A-3 engines, each producing 15 000 pounds of thrust for a total stage thrust of 90 000 pounds. An instrument unit on the forward end of the S-IV stage housed the vehicle's inertial

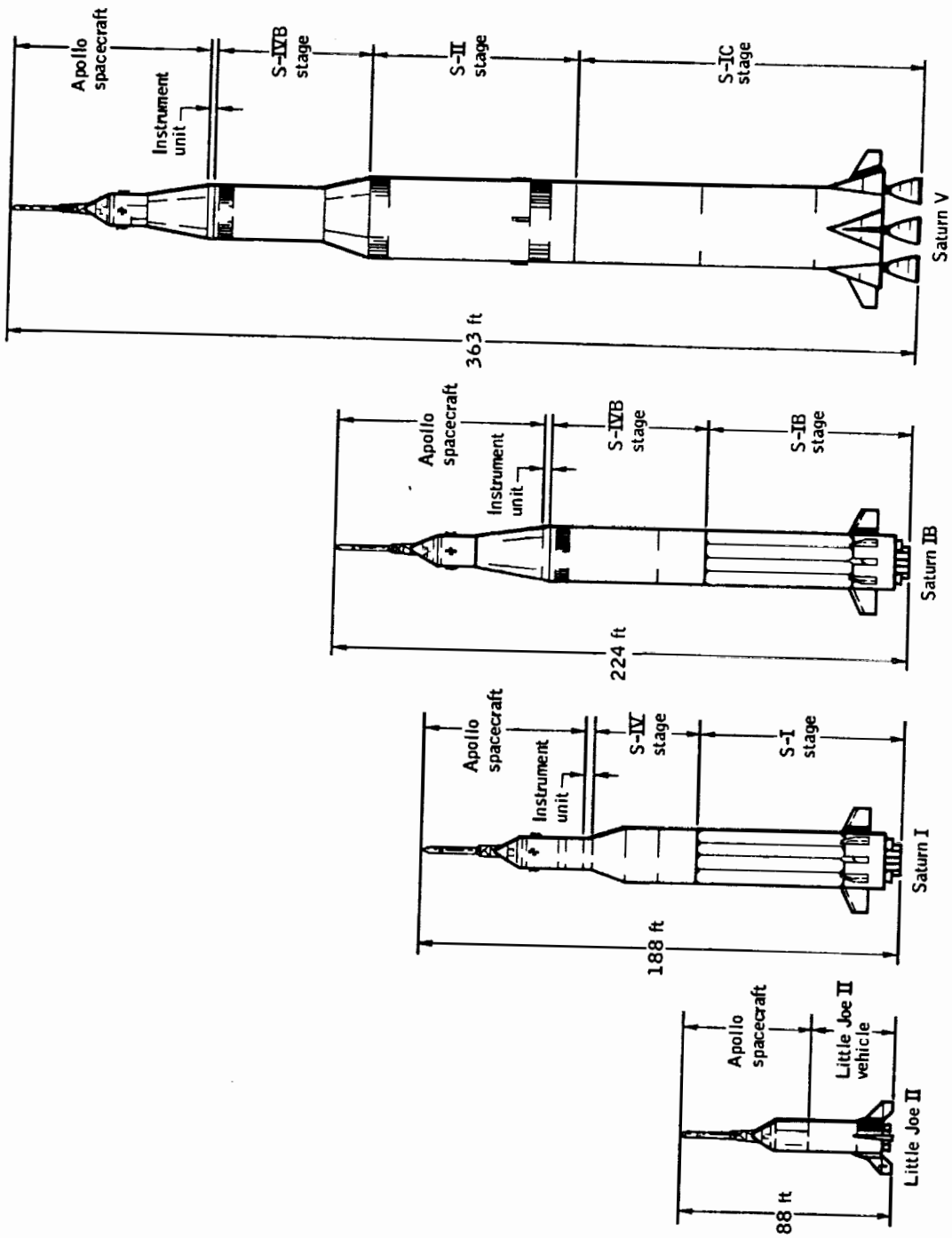

Figure 4-1.- Apollo launch vehicle configurations.

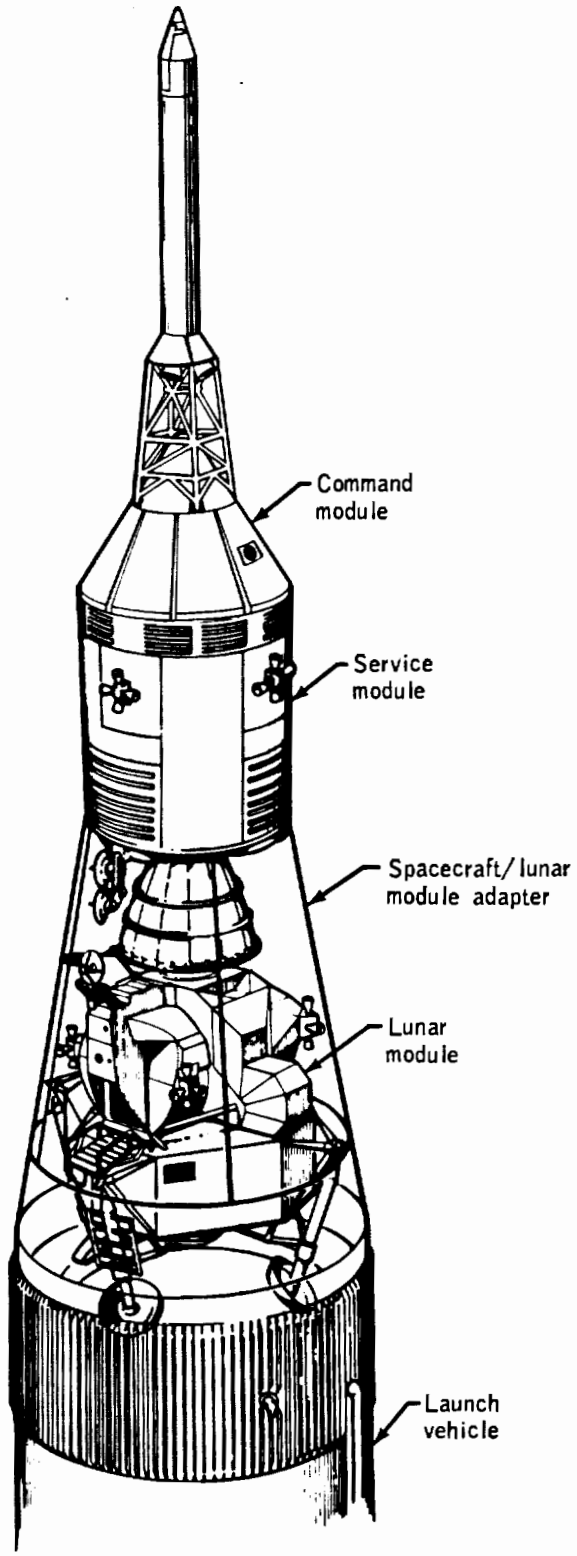

Figure 4-2.- Apollo launch configuration for lunar landing mission.

guidance and control equipment, instrumentation and measuring devices, power supplies, and telemetry transmitters. Thrust vector or path control of the S-I stage was by means of four gimbal-mounted outer engines moving in response to computer-generated commands in the instrument unit. The Saturn I, 188 feet in height and 21.7 feet in diameter, typically weighed 1 140 000 pounds when fully fueled.*

4.1.3 Saturn IB

The Saturn IB, also a liquid-propellant, two-stage rocket, was, for the most part, an uprated Saturn I. Construction of the first stage (S-IB) was similar to, but 2.4 inches shorter than the S-I stage. The eight H-1 engines were uprated to produce 200 000 pounds of thrust each for a total stage thrust of 1 600 000 pounds. The second stage (S-IVB) had a single J-2 engine, using liquid oxygen and liquid hydrogen to generate 225 000 pounds of thrust. The instrument unit attached to the forward end of the S-IVB stage performed the same functions as that of the Saturn I. The Saturn IB was 224 feet in height and 21.7 feet in diameter. The weight of the vehicle at launch was typically 1 300 000 pounds.*

4.1.4 Saturn V

The Saturn V was a liquid-propellant, three-stage rocket. The first stage (S-IC) had five engines, using liquid oxygen and RP-1. Each engine produced 1.5 million pounds of thrust. Thus, the S-IC stage generated 7.5 million pounds of thrust. The second stage (S-II) had five J-2 engines and produced 1 125 000 pounds of thrust. The third stage was an S-IVB, essentially the same as that of the Saturn IB. Similarly, the Saturn V instrument unit was basically the same as that of the Saturn IB. The Saturn V, 363 feet in height and 33 feet in diameter at the S-IC stage, typically weighed 6 500 000 pounds when fully fueled.*

4.1.5 Design and Development

The design safety factors for the Saturn vehicles were based originally on those required for an aircraft. These values were adjusted downward in view of the experience gained in the Mercury and Gemini programs and because of the proposed structure of the Saturn vehicles.

The design mission of the Saturn I was to place a 38 000-pound payload consisting of the Apollo boilerplate command module into a 100-mile orbit on a launch azimuth between 100° and 90° east of north from Cape Kennedy. On a secondary mission, a ballasted Jupiter nose cone contained a Q-ball transducer for measuring vehicle angle of attack. The major design criteria for the Saturn I were:

a. Minimum vehicle lift-off weight to thrust ratio

b. Man-rated vehicle

c. Self-supporting structure

d. Unipotential electrical structure

e. Mission achievement with one engine out in the first or second stage

f. Yield safety factor of 1.10 times design load

g. Ultimate safety factor of 1.40 times design load

The design mission for the Saturn IB was to place a 41 600-pound Apollo spacecraft into a 105-mile orbit at a launch azimuth of 70° east of north from Cape Kennedy. The major design criteria were the same as those for the Saturn I. The design mission for Saturn V was to place 250 000 pounds into a 100-mile orbit at a launch azimuth of 70° east of north from Cape Kennedy. Again, the major design criteria were the same.

*Vehicle heights and weights are for final configurations and include Apollo spacecraft payloads.

The testing program developed for the Saturn vehicles was designed to ensure a high degree of reliability and mission success. The degree to which it succeeded is demonstrated by the fact that, at the end of the Apollo program, the success records of the Saturn I, Saturn IB, and Saturn V vehicles were 100, 100, and 92 percent, respectively. Moreover, these results were achieved by launching far fewer research flights than had been the practice during the development of large missiles such as the Atlas and Titan, which preceded Saturn as the first carrier vehicles for U.S. manned flights. The Saturn I was declared operational after the seventh flight; the Saturn IB was certified for manned flight after only three flights; and the far more complex Saturn V was ready for launching its first manned payload after only two flights.

The concept of "all up" testing was instituted with the advent of the Saturn V. With this procedure, all three stages were flight tested on the first vehicle launched. The AS-501 (Apollo 4) vehicle, launched on November 9, 1967, was the first application.

The testing program for the Saturn vehicles was purposely designed to be conservative to ensure the highest reliability possible. The five essential phases were qualification, reliability, development, acceptance, and flight testing. Qualification testing assured that individual parts and subassemblies performed as required as a result of special tests that subjected parts to the vacuum, vibration, sound, heat, and cold levels that would be experienced in operational use. Reliability analysis consisted of determining the range of failures or margins of error for components. Development testing used "battleship" test stages of the vehicle to verify design features such as propellant loading, electrical continuity, and engine firing procedures. As a part of the developmental testing, a Saturn V test vehicle with an Apollo spacecraft in place was suspended in the 420-foot-high dynamic test stand at the Marshall Space Flight Center and shaken to simulate flight forces to determine vehicle bending modes and vibration frequencies. Acceptance testing included a functional checkout at the manufacturer's facility to ensure that the components or stage performed to design specifications. For example, ultrasonic techniques were used to inspect a fourth of a mile of welding and 5 miles of tubing in the Saturn V. The same technique was also used to verify the integrity of adhesive bonding in over 1 acre of such surfaces.

During the development of the Saturn V, a number of problems arose, the solution of which materially advanced the state of the art of design and manufacture of large rockets. Typical of these was the realization that the emergency detection system of the vehicle would not be effective in the case of an engine going out in the S-IC stage or an actuator of such an engine locking in the hardover position. The problem was solved by redesigning the stage control system and increasing structural tension capability at critical joints within the stage.

Several major problems that arose during manufacture were successfully solved. When conventional forming methods for producing large, curved panels with irregular cross sections proved insufficient for the size, shape, and tolerance demanded by the Saturn V, engineers developed special forming processes to meet the requirements. One of the great problems encountered during the development of propellant tanks was providing adequate insulation for liquid hydrogen at minus 423° F. The problem was solved by the development of a special polyurethane foam with the insulative properties of balsa wood. Although balsa wood had been an early, almost ideal candidate for such a job, it was difficult to obtain in the desired quantities, difficult to machine, and could not be found in a flawless state. Thus, imaginative materials engineering produced, in effect, a plastic substitute for flawless balsa wood. The plastic foam proved to be efficient, economical, and easy to shape.

In the course of the development of the Saturn vehicles, most operational problems had been foreseen. There were, of course, minor technical problems involved in the many mechanical, electrical, and pneumatic interfaces between the launch vehicle and its associated ground support equipment. In the case of the Saturn V, these were, for the most part, resolved through the use of a facilities model. The SA-500F vehicle was not meant to fly but was similar in every respect to a flight vehicle. Its purpose was to verify launch procedures, train launching crews, and develop checkout procedures. The SA-500F was rolled out from the Vehicle Assembly Building at Cape Kennedy on May 25, 1966.

4.1.6 Mission Performance

The mission performance of the Saturn vehicles proved that their design and manufacture were equal to the requirements placed upon them. The Saturn I vehicle made 10 flights between 1961 and 1965, all of which were successful. Similarly, the Saturn IB made five flights between 1966 and 1968, all of which were also successful. Of the 12 Saturn V flights through the end of the Apollo program, only one flight had a launch vehicle failure which precluded attainment of the primary mission objectives. On the Apollo 6 mission, an unmanned development flight, two of the second stage engines shut down early, and the third-stage engine failed to start after a programmed orbital coast period.

Relatively few Saturn V design changes were made from mission to mission because of the limited number of vehicles planned and built. Changes were made only to reduce weight, increase safety or reliability, or improve payload capability.

Typical of the early changes resulting from mission performance was the removal of air scoops from the S-IC stage of SA-502, the Apollo 6 launch vehicle, when it was found from the Apollo 4 flight that they were not needed and that their absence increased ground clearance at lift-off. Similarly, on the same vehicle, it was found that four ullage rockets were sufficient to seat propellants in the S-IVB stage; thus, four of the original eight were eliminated with a concomitant weight saving.

A major modification was made on SA-503, the Apollo 8 vehicle, as a result of the Apollo 6 mission. A longitudinal oscillation or "pogo" effect was experienced as a result of engine thrust variations coupling through propellant feed lines to the structure of the vehicle to produce a pronounced vibration. Helium gas was injected into the liquid oxygen prevalves of the suction lines to dampen the unwanted oscillations.

On SA-504, the Apollo 8 vehicle, a number of changes were made in the S-IC and S-II stages to reduce the vehicle weight and provide greater payload capacity. Typical of these were the redesign of the liquid oxygen tank of the S-IC stage to make it lighter and the uprating of the J-2 engine of the S-II stage from 225 000 to 230 000 pounds of thrust.

For the Apollo 15 mission (launch vehicle SA-510), an increased payload capability of about 5000 pounds was required. This increase resulted from the additional weight of consumables and hardware for supporting the longer duration lunar stay requirements of the J-series missions, as well as the addition of the scientific instrument module in the service module and the lunar roving vehicle. Many minor modifications were made to the launch vehicle and to the mission requirements to meet this payload increase. Part of this gain in payload capability came through uprating the five F-1 engines of the S-IC stage from 1 500 000 pounds to 1 522 000 pounds of thrust. Additional payload capability was gained by eliminating the four solid-propellant retromotors from the S-IC stage and by deleting the remaining four ullage motors from the S-II stage. In addition, the flight program of the instrument unit had to be changed to place the S-IVB stage into an earth parking orbit at 90 miles. No significant changes were made to the Saturn V for the two remaining missions, Apollo 16 and 17.

4.2 LITTLE JOE II PROGRAM

4.2.1 Introduction

From August 1963 to January 1966, a series of unmanned flight tests was conducted at the White Sands Missile Range to demonstrate the adequacy of the Apollo launch escape system and to verify the performance of the command module earth landing system. The launch vehicle used for four of these tests was the Little Joe II. The size of this vehicle is compared to that of the Saturn vehicles in figure 4-1. Its predecessor, the Little Joe, had been used in testing the launch escape system for the Mercury spacecraft. In addition to the Little Joe II flights, two pad abort tests were conducted in which the launch escape system was activated at ground level. Details of the six flights are given in appendix A.

The program was originally planned to be conducted at the U.S. Air Force Eastern Test Range at Cape Kennedy. However, because of a heavy schedule of high-priority launches at that facility, other possible launch sites were evaluated. Launch Complex 36 at the White Sands Missile Range, previously used for Redstone missile tests, was ultimately selected as the most suitable for meeting schedule and support requirements. Also, the White Sands Range allowed land recovery which was less costly and complicated than the water recovery procedure that would have been required at the Eastern Test Range or at the NASA Wallops Island facility.

The program was conducted under the direction of the Manned Spacecraft Center with joint participation by the prime contractors for the launch vehicle and spacecraft. The White Sands Missile Range administrative, range, and technical organizations provided the facilities, resources, and services required. These included range safety, radar and camera tracking, command transmission, real-time data displays, photography, telemetry data acquisition, data reduction, and recovery operations.

4.2.2 Launch Vehicle Development

Man-rating of the launch escape system was planned to be accomplished at minimum cost early in the Apollo program. Since there were no reasonably priced launch vehicles with the payload capability and thrust versatility that could meet the requirements of the planned tests, a contract was awarded for the development and construction of a specialized launch vehicle. Fabrication of detail parts for the first vehicle started in August 1962, and final factory systems checkout was completed in July 1963. The original fixed-fin configuration and a later version using flight controls are shown in figure 4-3.

The vehicle was sized to match the diameter of the Apollo spacecraft service module and to suit the length of the Algol rocket motors. Aerodynamic fins were sized to assure that the vehicle was inherently stable. The structural design was based on a gross weight of 220 000 pounds, of which 80 000 pounds was payload. The structure was also designed for sequential firing with a possible 10-second overlap of four first-stage and three second-stage sustainer motors. Sustainer thrust was provided by Algol solid-propellant motors. Versatility of performance was achieved by varying the number and firing sequence of primary motors (capability of up to seven) required to perform the mission. Recruit rocket motors were used for booster motors as required to supplement lift-off thrust. The configurations of the five vehicles flown are summarized in table 4-I.

A simplified design, tooling, and manufacturing concept was used to limit the number of vehicle components, reduce construction time, and hold vehicle costs to a minimum. Because overall weight was not a limiting factor in the design, overdesigning of primary structural members greatly reduced the number and complexity of structural proof tests. Whenever possible, vehicle systems were designed to use readily available off-the-shelf components that had proven reliability from use in other aerospace programs, and this further reduced overall costs by minimizing the amount of qualification testing required.

4.2.3 Spacecraft

The command and service modules used in this program evolved from the simple structure of boilerplate 6, representing only the proper aerodynamic shape, to the production spacecraft structure of airframe 002, a flight-weight Block I structure with crew couch struts, flight-weight heat shield, crew windows, and other Apollo flight hardware.

The launch escape system consisted of the major structures and systems shown in figure 4-4. The launch escape tower was attached to the command module by explosive bolts. For a normal tower jettison, the bolts were pyrotechnically severed and the tower jettison motor was ignited. For aborts requiring use of the launch escape system, the launch escape motor (and pitch control motor for low-altitude aborts) would have been fired to propel the command module away from the launch vehicle. After launch escape vehicle turnaround, the tower would have been separated from the command module by ignition of the explosive bolts and firing of the tower jettison motor.

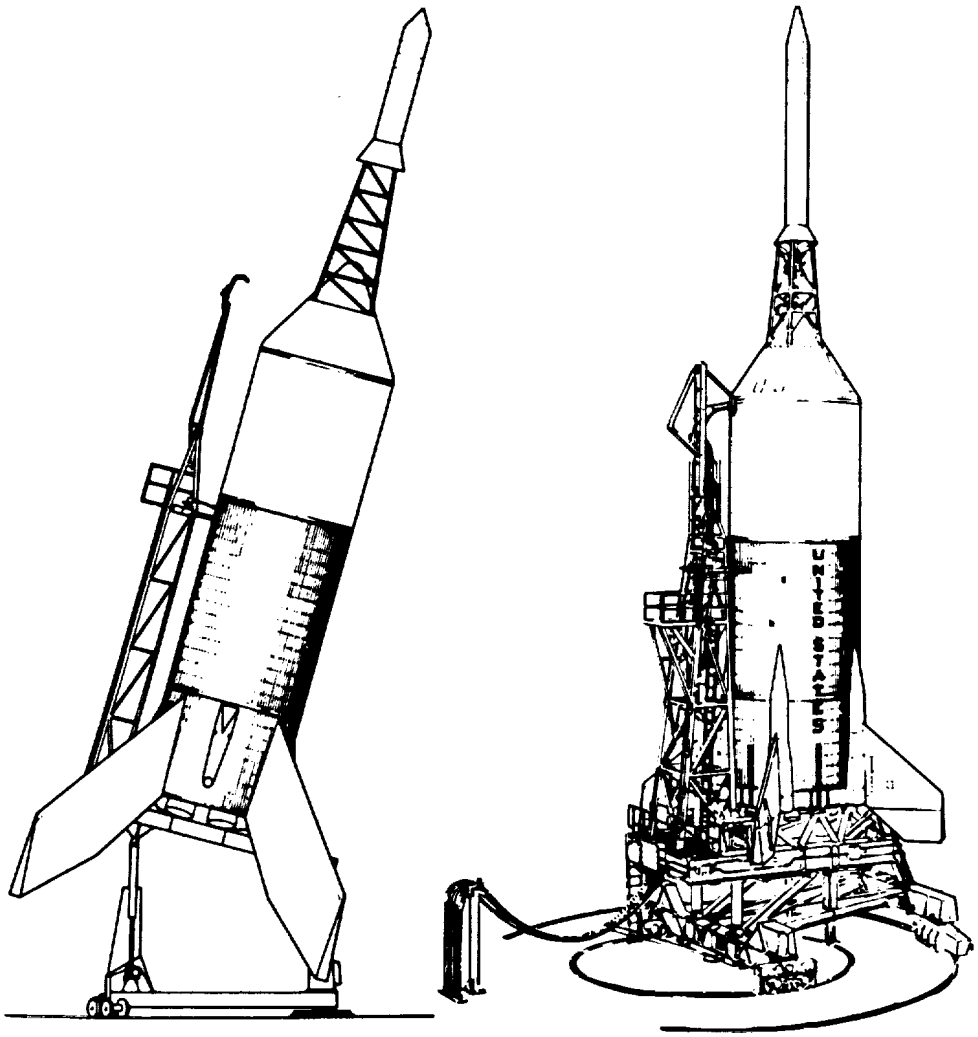

Original configuration

Final configuration

Figure 4-3.- Little Joe II vehicle.

TABLE 4-I.- LAUNCH VEHICLE CONFIGURATION SUMMARY

Item	[a]QTV	A-001	A-002	A-003	A-004
Launch weight, lb	57 165	57 939	94 331	177 189	139 731
Payload:					
Weight, lb	24 225	25 335	27 692	27 836	23 185
Ballast, lb	-	-	-	-	9361
Airframe:					
Weight including motors, lb	32 941	32 595	58 030	144 309	101 328
Ballast, lb	-	-	8609	5044	5867
Fixed fin	X	X	-	-	-
Controllable fin	-	-	X	X	X
Propulsion:					
First stage (Recruit)	6	6	4	-	5
First stage (Algol)	1	1	2	3	2
Second stage (Algol)	-	-	-	3	2
Attitude control:					
Pitch programmer	-	-	X	X	X
Pitchup capability	-	-	X	-	X
Reaction control	-	-	X	X	-
Aerodynamic control	-	-	X	X	X
RF command:					
Range safety destruct	X	-	X	X	X
Thrust termination and abort	-	X	-	-	-
Pitchup and abort	-	-	X	-	X
Abort	-	-	-	X	X
Electrical:					
Primary	-	-	X	X	X
Instrumentation	X	-	X	-	X
Instrumentation:					
RF transmitters	3	(b)	2	(b)	1
Telemetry measurements	66	3	58	13	39
Landline measurements	24	24	37	45	36
Radar beacon:					
Launch vehicle	X	-	-	-	-
Payload	-	X	X	X	X

[a]Qualification test vehicle.

[b]Located in payload.

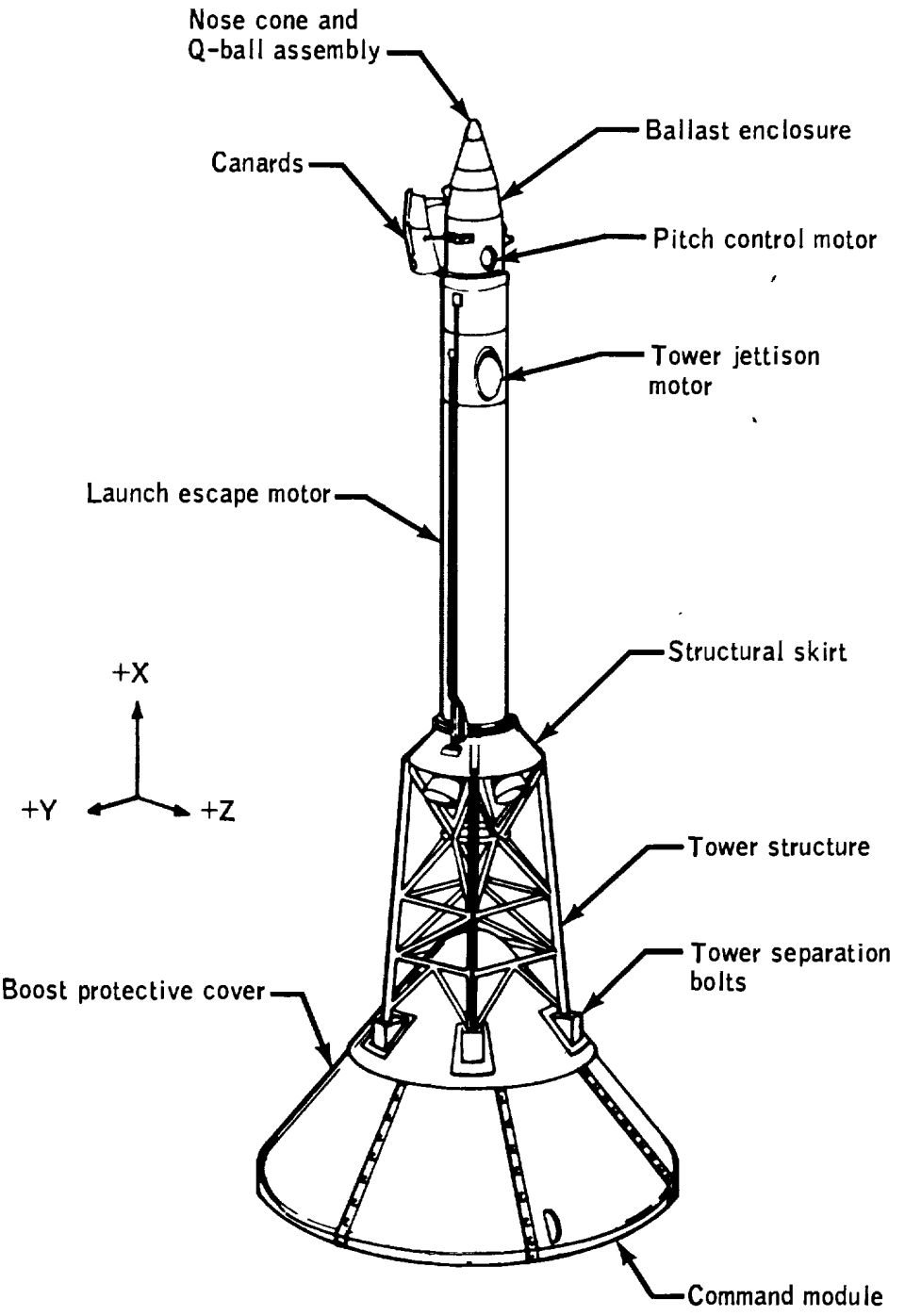

Figure 4-4.- Launch escape vehicle configuration for mission A-003.

Early in the flight testing phase of the Little Joe II program, data from other sources indicated that previously designed destabilizing strakes on the command module were ineffective in assuring a blunt-end-forward attitude following an abort. (The design of the parachute recovery system required that the forward heat shield and parachutes be deployed into the wake of the command module when descending at high velocities.) To assure the proper command module attitude for all abort conditions, two wing-like surfaces, called canards, were added to the forward end of the launch escape system (fig. 4-4). The canards were deployed by a pyrotechnic thruster acting through a mechanical linkage. The thruster also contained a hydraulic attenuator for control of the deployment speed and a mechanical lock to maintain the surfaces in the fully open position following deployment. The launch escape system was never required to be used during any of the Apollo missions; however, the tests conducted during the Little Joe II program demonstrated that the system would have performed its function successfully had it been required.

At about this same time in the program, severe abrasion of the command module windows was found to have been caused by the launch escape motor exhaust. Since visual references were required by Apollo crews in the event of an abort after launch escape tower jettisoning, a boost protective cover was designed to envelop the command module during the early boost stage of an Apollo mission. The cover was fabricated from fiberglass cloth to which an outer layer of cork was bonded. Windows were also installed to allow visibility from within the command module. The cover assembly was attached to the launch escape tower base and was separated from the command module when the tower was jettisoned.

4.2.4 Concluding Remarks

The Little Joe II launch vehicle proved to be very acceptable for use in this program. Two difficulties were experienced. The qualification test vehicle did not destruct when commanded to do so because improperly installed primacord did not propagate the initial detonation to the shaped charges on the Algol engine case. The fourth mission (A-003) launch vehicle became uncontrolled about 2.5 seconds after lift-off when an aerodynamic fin moved to a hardover position as the result of an electronic component failure. These problems were corrected and the abort test program was completed.

Minor spacecraft design deficiencies in the parachute reefing cutters, the drogue and main parachute deployment mortar mountings, and the command module/service module umbilical cutters were found and corrected before the manned Apollo flights began. However, all command modules flown achieved satisfactory landing conditions and confirmed that, had they been manned spacecraft, the crew would have survived the abort conditions.

4.3 COMMAND AND SERVICE MODULE DEVELOPMENT PROGRAM

4.3.1 Introduction

The Apollo program was, from the outset, planned as a multiphase program with each phase serving, to the extent possible, as qualification for subsequent phases. The phases were planned to overlap and were originally defined as follows.

The first phase was limited to manned, low-altitude, earth-orbital flights using a Saturn I launch vehicle. Contractor and subcontractor efforts emphasized detail design and analysis, preparation of detail specifications, development of special manufacturing techniques, and the fabrication of breadboards and flight test hardware. The spacecraft was designed to be capable of lunar landing and return.

The second phase consisted of circumlunar, lunar-orbital, and parabolic entry test flights using the Saturn-V-type launch vehicle for the purpose of further development of the spacecraft and operational techniques and for lunar reconnaissance.

The third phase consisted of manned lunar landing and return missions using either Nova-class launch vehicles or Saturn-V-type launch vehicles.

The spacecraft design concept at the initiation of the Apollo program was a vehicle capable of descending directly to the lunar surface. Thus, the decision in 1962 to use the lunar rendezvous technique had a major impact on the design. Since the direct landing capability was no longer needed, the propulsion requirements were changed to provide only for midcourse corrections, lunar-orbit insertion, and transearth injection. The new mission profile also necessitated revisions to the command module to incorporate provisions for rendezvous and docking with a lunar module and crew transfer between vehicles.

During the early conceptual design period, the need for a number of additional changes became evident. For instance, the original concept of employing a land landing system on the command module was discarded in favor of a water landing system, and the heat shield design was changed from one utilizing ablative tiles to one in which honeycomb cells were filled with ablative material. Because of the complexity of the program, the state-of-the-art development, and concurrent activities, these and other changes could not be accommodated with the existing facilities, test equipment, and special skills. As a result, a program definition study was conducted in 1964 to define the functional realignment of the command and service module systems that was mandatory for the lunar mission vehicles. The results dictated a two-phase development program whereby the command and service module would first be developed without the lunar mission capability (Block I) and subsequently redesigned to accommodate the lunar module and other systems advancements (Block II). The purpose in dividing the program was to test the basic structure and systems as quickly as possible, while providing the time and flexibility to incorporate changes. Thus, in addition to the incorporation of equipment for lunar missions, Block II spacecraft contained a great number of refinements and improvements of systems and equipment. Some of these were the result of continuing research, whereas some evolved from unmanned flights and ground tests.

4.3.2 Block I and Block II Hardware

4.3.2.1 Boilerplate spacecraft.- The first vehicles used in the test program were known as boilerplate spacecraft. These were pre-production spacecraft that were similar to their production counterparts in size, shape, mass, and center of gravity. These vehicles were used for parachute research and development, water drop tests, studies of stability characteristics, vibration tests, flight tests, and other purposes leading to the proper design and development of the actual spacecraft and its systems. Each boilerplate was equipped with instrumentation to permit recording of data for engineering study and evaluation.

4.3.2.2 Block I spacecraft.- The Block I spacecraft were limited-production flight-weight spacecraft used for flight systems development and qualification. The initial missions were conducted to verify production spacecraft structural integrity, systems operation, and systems compatibility. After the structure and systems tests were completed, a series of unmanned flight missions was conducted to confirm the compatibility of the spacecraft and launch vehicle and to evaluate prelaunch, mission, and postmission operations. A manned Block I spacecraft mission (originally designated AS-204 and later designated Apollo I) was planned to confirm the compatibility of the spacecraft and crew; however, the spacecraft was destroyed during a prelaunch test on January 27, 1967, and the crew, astronauts Virgil I. Grissom, Edward H. White II, and Roger B. Chaffee, were lost in the resulting fire. While an investigation of the accident was being conducted and corrective actions taken, there was a hiatus of about 18 months before another manned mission was ready.

4.3.2.3 Block I ground test vehicles and fixtures.- One boilerplate and several spacecraft modules were used in various ground tests at the manufacturer's facility and at the Manned Spacecraft Center to provide data on systems performance prior to flight testing.

Service propulsion system ground testing was accomplished with three test fixtures. The fixtures were unique platforms for the tests and were fully instrumented to record engine and propellant system performance through varied operating ranges. A service module having a complete flightworthy service propulsion system and electrical power system was used to demonstrate that the service module was compatible with all interfacing systems and structure and to evaluate the performance of the service propulsion system.